Water Research 209 (2022) 117864

Contents lists available at ScienceDirect

Water Research

journal homepage: www.elsevier.com/locate/watres

Reactions of amines with ozone and chlorine: Two novel oxidative methods to evaluate the N-DBP formation potential from dissolved organic nitrogen

Karim-Alexandre Essaïed [a], Lucy Victoria Brown [a,b], Urs von Gunten [*,a,c,d]

[a] School of Architecture, Civil and Environmental Engineering (ENAC), Ecole Polytechnique Fédérale de Lausanne (EPFL), Lausanne 1015, Switzerland
[b] Department of Chemistry, University of York, Heslington, York YO10 5DD, United Kingdom
[c] Eawag, Swiss Federal Institute of Aquatic Science and Technology, Überlandstrasse 133, Dübendorf 8600, Switzerland
[d] Institute of Biogeochemistry and Pollutant Dynamics, ETH Zürich, Zürich 8092, Switzerland

ARTICLE INFO

Keywords:
Ozone
Chlorine
Dissolved organic nitrogen
Nitrate
Chloramine
Disinfection by-products

ABSTRACT

The composition of oxidant-reactive dissolved organic nitrogen (DON) is poorly characterized, although its ozonation is likely to form a great variety of disinfection by-products containing a nitrogen-oxygen bond (N-DBPs). In this study, two chemical oxidation procedures were developed: continuous ozonation at pH 7.0 and free available chlorine (FAC) titrations at pH 9.2. The formation of two oxidation products (nitrate (NO_3^-) and chloramines, respectively) was used to quantify and characterize oxidant-reactive nitrogenous moieties in DON. In addition, batch experiments were conducted to study the NO_3^- yields of 30 selected nitrogenous model compounds upon ozonation. The NO_3^- yields of 12 primary and secondary amines were highly variable (17–100%, specific ozone dose of 20 mol_{O3}/mol_N), 7 amino acids had high NO_3^- yields (≥90%), and tertiary amines as well as pyrrole, acetamide and urea had low NO_3^- yields (≤15%). The mechanisms of NO_3^- formation were further examined with benzylamine and *N*-methylbenzylamine as model compounds. Our results show that nitroalkanes are the last intermediate products before the formation of NO_3^-, both for primary and secondary amines. The presence of an electron-withdrawing group in the vicinity of the N-atom facilitates the formation of NO_3^- from nitroalkanes. Therefore, the formation of NO_3^- is attributed to amino acids and activated primary and secondary amines. In contrast, all primary and secondary amines were transformed to chloramines upon chlorination, which was determined by a novel oxidative titration with chlorine. To further support the selectivity of this assay, it was demonstrated by derivatization of amine moieties that chloramine formation could be inhibited. 13–45% of the DON of 4 dissolved organic matter isolates and 2 wastewater effluents formed NO_3^- and 0–39% formed chloramines, indicating that the potential for N-DBP formation is high ($\mu M_N/mg_C$-level). From differences in the formation of NO_3^- and chloramines the nature of the precursors can be hypothesized (e.g., activated or non-activated primary and secondary amines, partially oxidized nitrogenous compounds). This study highlights the capacity of two novel methods to characterize the oxidant-reactive DON fraction. Our results suggest that this fraction is significant and could form a variety of potentially toxic N-DBPs.

1. Introduction

Dissolved organic matter (DOM) is a complex mixture of heterogeneous chemical structures. It is ubiquitous in all water types, from source water (natural organic matter, NOM) to wastewater effluents (effluent organic matter, EfOM) (Leenheer and Croué, 2003; Shon et al., 2006). Its electron-rich moieties such as phenolic compounds, alkenes and amines are recognized as the principal consumers of chemical oxidants (e.g., ozone and chlorine) applied in drinking water and wastewater treatment (von Gunten, 2018), and react through various pathways (Deborde and von Gunten, 2008; Lim et al., 2019; Tekle-Röttering et al., 2020; von Sonntag and von Gunten, 2012). As a consequence, disinfection by-products (DBPs) are formed during primary disinfection/oxidation and final disinfection during distribution of drinking water (Rosario-Ortiz et al., 2016) or before discharge/reuse of wastewater. Many DBP classes have been studied, such as trihalomethanes (THMs), haloacetic acids (HAAs), haloacetonitriles (HANs), haloacetaldehydes, *N*-nitrosamines, halonitromethanes (HNMs), etc., each having specific

* Corresponding author.
E-mail address: urs.vongunten@eawag.ch (U. von Gunten).

https://doi.org/10.1016/j.watres.2021.117864
Received 4 August 2021; Received in revised form 5 November 2021; Accepted 9 November 2021
Available online 13 November 2021

molecular structures and toxicities (von Gunten et al., 2010; Krasner, 2009; Krasner et al., 2006; Li and Mitch, 2018; Mitch and Sedlak, 2002; Plewa et al., 2004; Richardson et al., 2007). In particular, nitrogenous DBPs (N-DBPs) are of increasing concern. Research suggests that some halogenated N-DBPs (e.g., HNM, HAN) could be more toxic than their carbonaceous analogues such as THMs or HAAs (Council, 2012; Muellner et al., 2007; Plewa et al., 2004; Stalter et al., 2016; Wagner and Plewa, 2017). Considerably less information is available on the formation of non-halogenated N-DBPs during ozonation with knowledge gaps about (i) the DON composition (serving as N-DBP precursors) and (ii) the mechanisms of reactions between DON moieties and ozone (leading to the formation of N-DBPs).

The heterogeneous nature of the DON constitutes a vast array of N-DBP precursors. DON is a mostly unresolved heterogeneous mixture, mainly composed of compounds originating from excretions of organisms or degradation (Jørgensen, 2009). Amino acids have been the most studied DON compounds and they generally represent 10–20% of the freshwater DON (Dotson and Westerhoff, 2009; Sipler and Bronk, 2015; Westerhoff and Mash, 2002). Other organic compounds such as amino-sugars (in peptidoglycan or chitin), dissolved nucleotides from RNA/DNA strands (containing purine), and their metabolites (urea, humic substances, D-amino acids, diaminopimelic acid, glucosamine and methylamines) also represent a significant fraction of the freshwater DON (Jørgensen, 2009; Jørgensen et al., 2003; Pehlivanoglu-Mantas and Sedlak, 2006). It is expected that the DON concentration in drinking water sources will increase due to eutrophication, run-off events, and potable water reuse (Council, 2012; Delpla et al., 2009; Gerrity et al., 2013; Graeber et al., 2015; Marron et al., 2019; Pehlivanoglu-Mantas and Sedlak, 2006; Sedlak, 2014). To this end, the chemical composition of wastewater effluent DON has been investigated, with concentrations generally in the range of 47–350 μM as N (Liu et al., 2012; Pehlivanoglu-Mantas and Sedlak, 2006). About 10–20% are composed of amino acids, <5% of chelating agents (e.g., EDTA, NTA), 10% of humic substances from source water, and <<0.1% of other N-containing micropollutants (Parkin and McCarty, 1981; Pehlivanoglu-Mantas and Sedlak, 2006; 2008). Overall, only a small fraction of the DON compounds has been identified (Pehlivanoglu-Mantas and Sedlak, 2006).

Ozone reacts with electron-rich amine moieties (Lim et al., 2019; Tekle-Röttering et al., 2020) by an initial addition at the lone electron pair of the nitrogen to form an ozone adduct $R–N^{+}–O–O–O^{-}$, which rapidly decomposes, mainly by losing $^{1}O_2$ (Lim et al., 2019; von Sonntag and von Gunten, 2012). For primary and secondary amines, the corresponding alkylhydroxylamine is then formed, which is rapidly further oxidized to nitro-products (Lim et al., 2019; Shi and McCurry, 2020). Nitromethane has been identified during ozonation of various model amine compounds, DOM isolates and wastewater (McCurry et al., 2016; Shi and McCurry, 2020). For tertiary amines, the main end products are *N*-oxides (Lim et al., 2019; Muñoz and von Sonntag, 2000; Zimmermann et al., 2012). It has also been demonstrated that ozonation of some aliphatic amines, DOM isolates and wastewater effluents forms nitrate (Song et al., 2017; de Vera et al., 2017), which is the endpoint of nitrogen oxidation. However, so far it is inconclusive which factors influence the nitrate formation yields. Comparatively, organic primary and secondary amines in their neutral form react with chlorine to quickly form the corresponding chloramines by electrophilic substitution (Deborde and von Gunten, 2008; Heeb et al., 2017; Wajon and Morris, 1982). At pH 7, organic amines exert significant second-order rate constants for the reactions with chlorine (10^3 - 10^4 $M^{-1}s^{-1}$) (Heeb et al., 2017). These chloramines can be detected by photometric methods targeting the total chlorine concentration (Aieta et al., 1984; Pinkernell et al., 2000), which possibly enables a quantification of the total amine concentration in DOM.

An assessment of the formation of N-DBPs during ozonation is therefore dependant on the understanding of the ozonation mechanisms and the nature of the precursors. To overcome these difficulties, new methods are required to identify and quantify the precursors of N-DBPs in DON. The aim of this study was to develop two novel assays using controlled oxidation conditions: (i) free available chlorine (FAC) titrations at pH 9.2 with the formation of chloramines and (ii) DON oxidation to nitrate by ozonation at pH 7.0. These methods rely on the pH dependance of the apparent second-order rate constants (k_{app}) for the reaction of chlorine and ozone with the major functional groups in DOM (Fig. 1a and b). Controlling the oxidation conditions can narrow down the diversity of target functional groups that react with the two selected oxidants. Chloramines and nitrate are two independent and easy to quantify parameters that are formed during the proposed controlled oxidations. They gauge the potential of N-DBP formation from the reactions of DON with ozone. These methods were optimized and tested with numerous model compounds, four NOM/EfOM isolates and two wastewater samples. Furthermore, a kinetic and mechanistic assessment of the nitrate formation during reactions of amines with ozone was carried out with 30 selected model compounds.

2. Material and methods

2.1. Chemicals and NOM/EfOM isolates

Chemicals used in this study are listed in Table S1 of the Supporting Information (SI), together with their suppliers and purities. Standard DOM isolates (i.e., Suwannee River Natural Organic Matter (SRNOM), Suwannee River Fulvic Acid (SRFA) and Upper Mississippi River Organic Matter (UMROM)) were obtained from the International Humic Substances Society (IHSS). Additionally, a wastewater effluent organic matter isolate (EfOM-CH) was obtained from the Université de Poitiers. Relevant physico-chemical characteristics of these isolates are provided in Tables S2 and S3 (SI).

2.2. Water samples

Synthetic water samples were prepared by dissolving a model compound or a standard NOM/EfOM isolate in ultra-pure water (Milli-Q water, Millipore, Merck, Germany; resistivity: 18.2 MΩ·cm at 25°C; TOC: 2 ppb). Before each experiment, the DOC concentration of a synthetic water containing a standard NOM/EfOM isolate was spectrophotometrically standardized with the procedure described in Text S1 (SI). Wastewater samples were obtained from the wastewater treatment plant "ARA Thunersee" (Thun, Switzerland). Samples were collected in amber glass bottles at two different treatment stages: (i) after the biological treatment (WWTA, including nitrification); (ii) after treatment for micropollutant removal (WWTB, powdered activated carbon and sand filtration (PAC + SF)). On the same day, they were filtered on a 2.7 μm glass microfiber filter (Whatman) and a 0.45 μm nylon membrane (Membrane Solutions), and stored in a refrigerator before use. Table S4 (SI) summarizes their main water quality parameters.

2.3. Preparation of ozone and chlorine stock solutions

For kinetic and batch dosage experiments, ozone gas was produced by a CMG 3–5 ozone generator (Innovatec) supplied with O_2 gas (Alphagas 2 O_2 99.9995%) at 12 and 13 L/h. The gas was passed through a phosphate buffer trap (0.5 M, pH 6), before continuous sparging through 500 mL ultra-pure water chilled in an ice bath until ozone saturation (1.1–1.2 mM). The ozone stock solution was spectrophotometrically standardized prior to use, by measuring the absorbance of a mixture of ozone stock (1 mL) and phosphoric acid (50 mM, 2 mL) in a 1 cm quartz cell ($\epsilon_{O_3,260\ nm}$= 3'200 $M^{-1}cm^{-1}$ von Sonntag and von Gunten, 2012). For continuous ozonation, ozone gas was produced by a LAB2B ozone generator (Triogen) supplied with O_2 gas (Alphagas 2 O_2 99.9995%).

A 40 mM stock solution of FAC was prepared from a commercial sodium hypochlorite solution in ultra-pure water. The commercial sodium hypochlorite solution and the FAC stock solution were

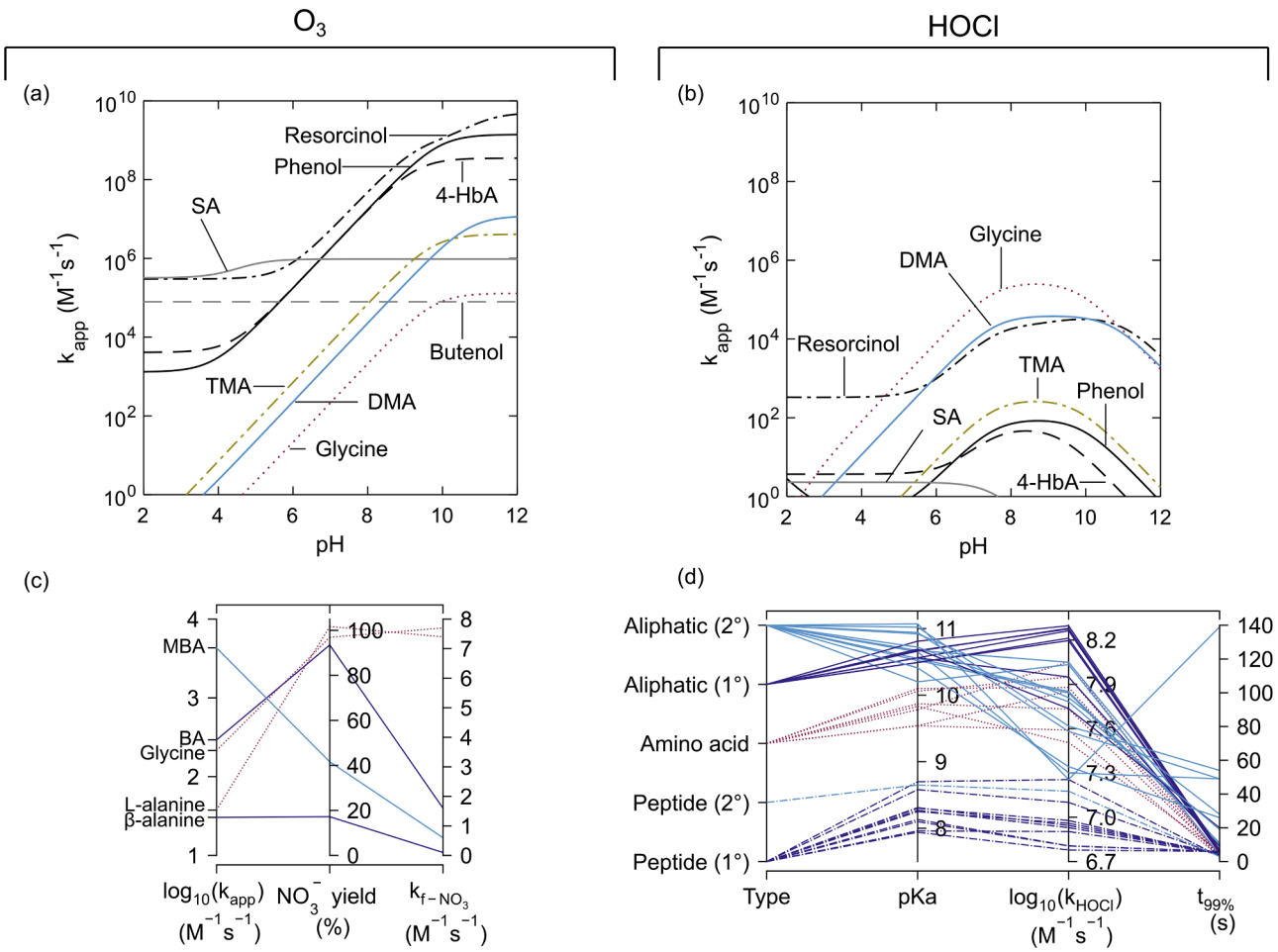

Fig. 1. (a, b) Apparent second-order rate constants (k_{app}) as a function of the pH, for the reactions of (a) ozone and (b) chlorine with model compounds: phenolic compounds (phenol, resorcinol, 4-hydroxybenzoic acid (4-HbA)), alkenes (sorbic acid (SA), butenol) and amines (glycine, dimethylamine (DMA) and trimethylamine (TMA)). (c) Parallel category plot for the ozonation of 5 selected model amine compounds (*N*-methylbenzylamine (MBA), benzylamine (BA), glycine, L-alanine and *β*-alanine), comparing their $\log_{10}(k_{app})$ with their NO_3^- yield (%) and the second-order rate constant of NO_3^- formation (k_{f-NO_3} ($M^{-1}s^{-1}$), Text S6, SI), at pH 7.0. The last two parameters were obtained from kinetic experiments for which the results and experimental conditions are reported in Figures S2 and S3 and Table S6 (SI). (d) Parallel category plot for the chlorination of 37 selected model amine compounds, comparing their pK_a and $\log_{10}(k_{HOCl})$ with the time needed to abate at least 99% of their initial concentration ($t_{99\%}$). This last parameter was calculated by kinetic simulations performed with a software architecture described in Figure S1 (SI). Modeling conditions: pH 9.2, $[HOCl]_0 = 15$ μM, $[amine]_0 = 10$. Rate constants and pK_a were obtained from (von Sonntag and von Gunten, 2012) and (Deborde and von Gunten, 2008) for O_3 and HOCl, respectively. Texts S5 and S9 (SI) describe the calculations for k_{app}.

spectrophotometrically standardized prior to use, in basic conditions and in a 1 cm quartz cell ($\epsilon_{OCl^-,292\ nm}$= 350 $M^{-1}cm^{-1}$ (Hand and Margerum, 1983)).

2.4. Nitrate formation during ozonation

2.4.1. Kinetic experiments with model compounds

The kinetics of NO_3^- formation were studied for 4 model compounds: benzylamine (primary amine), *N*-methylbenzylamine (secondary amine), L-alanine (*α*-amino acid) and *β*-alanine (*β*-amino acid) by following (1) the ozone decay and (2) the NO_3^- formation, for 90 min, in 20-fold stoichiometric molar excess of ozone, at pH 7. A solution of model amine (20 μM) and *tert*-butanol (*t*-BuOH, a hydroxyl radical scavenger; 20 mM) in phosphate buffer (10 mM, pH 7) was added to a 250 mL glass bottle equipped with a Dispensette III BottleTop dispenser (BrandTech) (Hoigné and Bader, 1994). The ozone stock solution was added below the liquid level through Teflon tubing ($[O3]_{t=0\ s} \approx$ 400 μM), using a glass syringe, and the solution stirred for 60 s. At specified time intervals (but not before 60 s), a 1 mL sample was taken and added to a vial containing indigo (0.25 mL, 2 mM) and phosphate buffer (0.25 mL, 20 mM, pH 2), to measure ozone by the indigo method (Section 2.6.3). After a delay of 5 s, a second 1 mL sample was transferred to a vial containing 10 μL 3-buten-2-ol (136 mM) to rapidly quench residual ozone (Text S2, SI). This sample was used to quantify NO_3^- by ion chromatography (IC, Section 2.6.1) without interference of indigo. The procedure was repeated in duplicate for each model compound.

2.4.2. Batch dosage experiments with model compounds for mechanistic investigations

Batch ozonation experiments were performed with 30 selected model compounds (Table S5, SI) to investigate the yields and mechanisms of NO_3^- formation. They were conducted in amber borosilicate glass vials containing one of the model nitrogenous precursors (50 μM), phosphate buffer (5 mM, pH 7.0), ultra-pure water and *t*-BuOH (20 mM). Appropriate volumes of an ozone stock solution were added last using a glass syringe, to obtain specific molar ozone:amine ratios (between 0 and 20) in a final volume of 15 mL. The vials were sealed with Teflon-lined septum caps and left to react for 24 h at room temperature before sparging any potential residual ozone with N_2 gas. The quenched samples were analyzed for nitrate by IC-UV (Section 2.6.1). For 3 model amines (benzylamine, *N*-methylbenzylamine and *N,N*-dimethylbenzylamine), other expected transformation products (TPs) were also

quantified by HPLC-UV and GC–MS/MS (Section 2.6.1) to further investigate the mechanism of nitrate formation.

2.4.3. Continuous ozonation

For standard NOM/EfOM and wastewater samples, continuous ozonation experiments were performed to determine (1) the NO_3^- evolution and (2) the maximum NO_3^- formation under high ozone excess conditions. 250 mL of ultra-pure water with NOM/EfOM isolates (DOC $\approx$ 10 mg_C/L, spectrophotometrically standardized) or 150 mL of ultra-pure water with 100 mL of wastewater sample (dilution factor: 2.5), each containing phosphate buffer (10 mM, solution pH 7.00 $\pm$ 0.05) and *t*-BuOH (100 mM) were continuously stirred in a GLS 80 glass reactor (Duran), equipped with a multiple gas-tight distributor PTFE cap, to accommodate 4 tubes (Fig. 2a). At t = 0 s, an O_2/O_3 gas mixture was continuously bubbled (0.5 L/min) in the sealed reactor through a Teflon tube connected to a frit. A liquid circulation loop entirely made of Teflon tubes was mounted between the reactor and a 0.5 cm flow-through quartz cell to continuously monitor and record the total absorbance of the solution at λ = 260 nm (reported as $(A_{260}/A_{260,\ max})_{tot}$), with a Shimadzu UV-1800 spectrophotometer. A peristaltic pump (flow rate: 6 mL/min, i.e., hydraulic residence time: 4 s in the cell) was placed after the spectrophotometer, and equipped with a thermoplastic elastomer (TPE) tube (PharMed BPT NSF-51), which has excellent ozone resistance. At specified time intervals, 500 µL of solution were collected for nitrate analysis (Section 2.6.1) with a gas-tight glass syringe through a T-piece and a valve installed on the circulation loop. Residual ozone was immediately quenched by an excess of sulfite ($[SO_3^-]_{final} \geq$0.8 mM, Text S2, SI). At less frequent time intervals, 2.5 mL of solution were collected and ozone was immediately sparged with N_2 gas. The absorbance at λ = 260 nm of the sparged solution was separately measured in a 0.5 cm quartz cell and reported as $(A_{260}/A_{260,0})_w$, i.e., the residual absorbance of the analyzed water not caused by ozone. Ozone exposures (OE, Ms) were calculated as

$$OE = \int_{t=0}^{120\ min} A_{260,O_3}(t)\cdot((3200\,L/(mol\cdot cm))\cdot(0.5\,cm))^{-1}\ dt$$

with $A_{260,O_3}(t) = A_{260,tot}(t) - A_{260,w}(t)$, a fitted function describing the absorbance of ozone over time (0–120 min) as the difference between the total absorbance of the solution and the absorbance of the water matrix only, at 260 nm

2.5. Chloramine formation during chlorination

2.5.1. Kinetic simulations

To evaluate the reaction time needed to transform amines to chloramines, 37 model amines were selected (with known species-specific second-order rate constant (k_{HOCl}) and pK_a at 25°C) from a database (Deborde and von Gunten, 2008). A software architecture linking Matlab with Kintecus (Figure S1, SI) was built to perform kinetic simulations to conveniently find the time needed to transform 99% of each amine to chloramines ($t_{99\%}$). Modeling conditions were chosen as follows: pH 9.2, $[amine]_0$ = 10 µM, $[HOCl]_0$ = 10, 12, 15, 20, 30 and 40 µM.

2.5.2. Oxidative FAC-titration

To perform oxidative titrations (Fig. 2b), increasing chlorine doses ($[FAC]_{t=0}$ = 0 to 40 µM) were added to a series of batch reactors (10 mL) containing a model compound (10 µM, unless indicated otherwise), or a NOM/EfOM isolate (DOC = 5 mg_C/L) or wastewater (Table S4, SI), and a

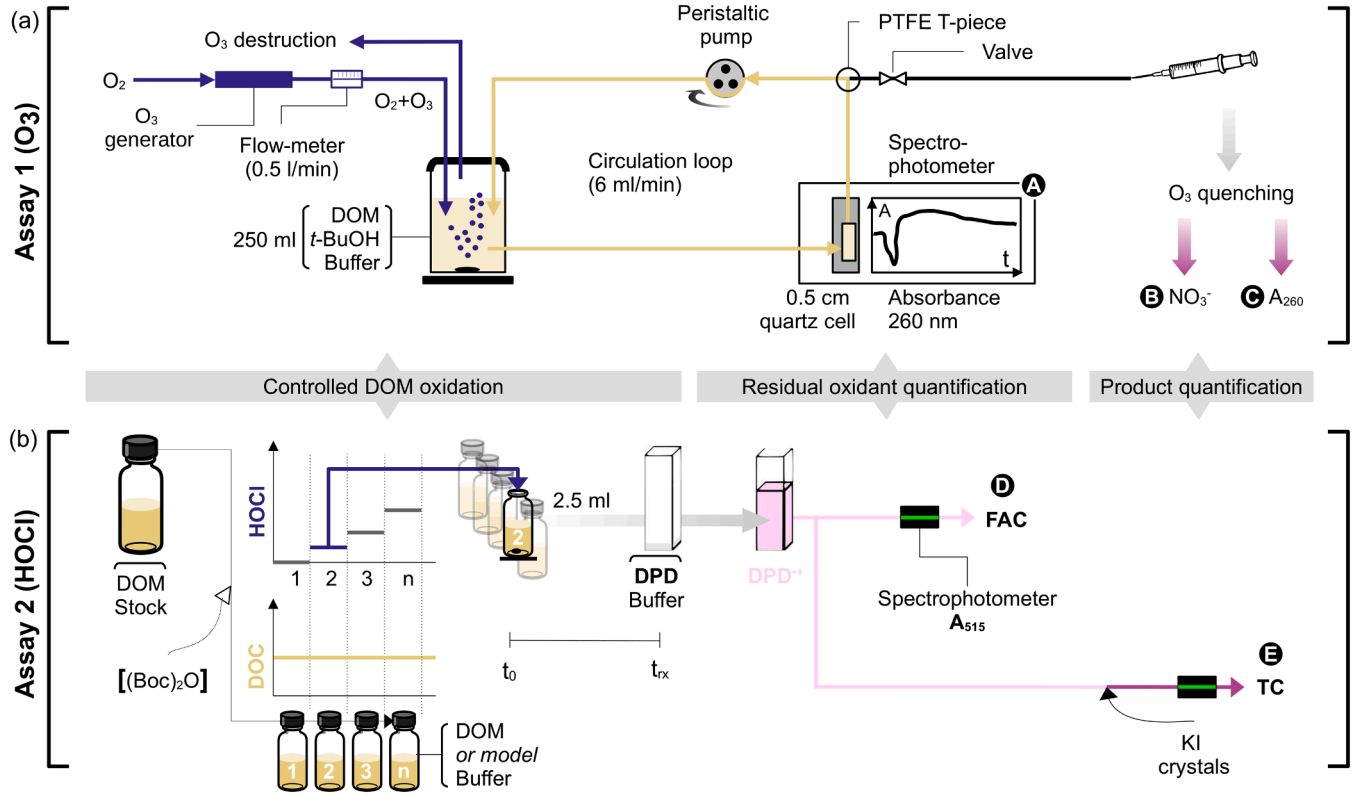

Fig. 2. Schematic representation of the experimental setups for (a) the continuous ozonation experiments and (b) the oxidative FAC-titrations. (a) Monitoring parameter A: the evolution of the reaction was continuously monitored by measuring the absorbance of the solution (λ=260 nm, optical path length = 0.5 cm). Monitoring parameter B: at selected reaction times, 0.5 mL of solution was withdrawn with a glass syringe and NO_3^- was quantified by IC-UV analyses. Monitoring parameter C: at less frequent reaction times, 2.5 mL of solution were collected to measure its absorbance at λ=260 nm, after ozone purging with N_2. (b) Monitoring parameters D and E: final concentrations of FAC and TC were spectrophotometrically quantified by the DPD method, for increasing HOCl doses (reactors 1 to n); the same procedure was applied with and without $(BOC)_2O$ derivatization.

carbonate buffer (5 mM, pH 9.2). After a selected reaction time (t_{rx}, determined by kinetic simulations), 2.5 mL of sample were immediately transferred to a 1 cm quartz cell containing 125 μL of a *N,N*-diethyl-*p*-phenylenediamine (DPD) solution and 125 μL of a phosphate buffer (0.22 M, pH 6.3). $[FAC]_{t=trx}$ and total chlorine ($[TC] = [FAC]_{t=trx} + [chloramines\ formed]_{t=trx}$) were quantified by the DPD colorimetric method (Section 2.6.2).

2.5.3. $(BOC)_2O$-derivatization of primary and secondary amines

A derivatization procedure was adopted to selectively block the reactivity of primary and secondary amines towards chlorination, by transforming them into carbamates. It was based on a method using di-*tert*-butyl dicarbonate $(BOC)_2O$ as protecting agent (Einhorn et al., 1991). The detailed procedure is described in Text S3 (SI).

2.6. Analytical methods

2.6.1. Quantification of amines and their TPs

Benzylamine (BA), *N*-methylbenzylamine (MBA), *N,N*-dimethylbenzylamine (DMBA) and their ozonation TPs, i.e., *N,N*-dimethylbenzylamine *N*-oxide, nitromethylbenzene, benzaldehyde oxime and *N*-methyl-1-phenylmethanimine oxide were measured by high pressure liquid chromatography (HPLC) equipped with an UV detector. They were identified by retention time comparison with commercial standards. Nitrate was measured by ion chromatography (IC) with UV detection at 220 nm. Nitromethane was measured by gas chromatography and tandem mass spectrometry (GC–MS/MS) after a liquid-liquid extraction. Chromatographic conditions, calibrations and limits of quantification are provided in Text S4 (SI).

2.6.2. Quantification of FAC and total chlorine (TC)

FAC concentrations were measured by the DPD colorimetric method described elsewhere (Baird et al., 2017; Rodier et al., 2016). DPD is oxidized by FAC to the Würster dye ($DPD^{\bullet+}$), which can be spectrophotometrically quantified at λ = 510 nm ($\epsilon_{DPD^{\bullet+},510\ nm}$ = 19'800 $M^{-1}cm^{-1}$, Bader et al., 1988) in a 1 cm quartz cell. By the subsequent addition of potassium iodide (KI) crystals, total chlorine (TC = FAC + mono- + dichloramines) was also quantified. The LOD and LOQ of the DPD method were 0.75 μM and 2.28 μM, respectively.

2.6.3. Quantification of ozone

The indigo method was used to quantify the ozone concentration (Bader and Hoigné, 1981). Rapid reaction between excess indigotrisulfonate and residual ozone at pH = 2 (1:1 molar ratio) causes discoloration of the initial blue indigo solution, for which the absorbance was recorded at λ = 600 nm ($\epsilon_{indigo,600\ nm}$ = 20'000 $M^{-1}s^{-1}$, Bader and Hoigné, 1981) in a 1 cm quartz cell. This allowed quantification of ozone concentrations as a function of reaction time in kinetic experiments.

2.6.4. Quantification of DON in water samples

For the wastewater samples, DON was determined by size-exclusion chromatography coupled to UV organic carbon and nitrogen detection (SEC-UV-OCD-ND) (Chon et al., 2013). Samples were dialysed (cellulose ester dialysis tubes Biotech, diameter 15 mm, 0.1–0.5 kDa molecular weight cutoff, Spectrum Laboratories) prior to SEC-UV-OCD-ND to minimize interference from inorganic nitrogen (NO_3^- and NH_4^+). For the NOM isolates, the elemental nitrogen content published by the IHSS was used (Table S3, SI).

2.6.5. Quantification of other wastewater quality parameters

Alkalinity, DOC, total dissolved nitrogen (TDN), NO_3^-, NO_2^-, NH_4^+ and pH were determined at Eawag (Dübendorf, Switzerland) using methods described in Table S4 (SI).

3. Results and discussion

3.1. Assessment of the nitrate formation during ozonation of model compounds

Before measuring the nitrate formation during ozonation of DOM/EfOM samples, the relevance and extent of nitrate as an oxidation end product had to be evaluated. To strengthen the current mechanistic knowledge, three aspects were studied with several model nitrogenous compounds: (1) the temporal evolution of NO_3^- formation with 4 model amines (kinetic experiments); (2) the yields of NO_3^- formation with 30 model amines (dosage experiments); (3) the mechanisms of NO_3^- formation with 3 aliphatic amines (dosage experiments).

3.1.1. Kinetics of nitrate formation from model amine compounds

To study the evolution of nitrate during ozonation, kinetic experiments were performed with BA, MBA, L-alanine and *β*-alanine and the results were compared with previously published data for glycine (de Vera et al., 2017). These compounds were chosen after evaluation of their apparent second-order rate constants (k_{app}, Text S5, SI) at pH 7, which ranged over 2 orders of magnitude (Table S6, SI).

O_3 was completely consumed within 90 min for each of the compounds (Figure S2, SI), comparable to glycine under similar conditions (de Vera et al., 2017). The ozone exposures were between 0.32 and 0.39 M·s (256–312 mg·min/L), but higher for *β*-alanine (0.57 M·s or 456 mg·min/L). The second-order rate constants for NO_3^- formation ($k_{f-NO_3^-}$, as defined in Text S6 and Figure S3, SI) and NO_3^- yields were determined, based on the profiles of O_3 decay and NO_3^- formation over time.

In Fig. 1c, k_{app}, NO_3^- yields and $k_{f-NO_3^-}$ are compared in parallel for the five target compounds. Clearly, no correlation exists between k_{app} and the NO_3^- yields nor between k_{app} and $k_{f-NO_3^-}$. This suggests that the nitrate formation kinetics and yields are not controlled by the initial ozone attack but by further reactions involving intermediate transformation products. The chemical structures of these intermediates could be a key parameter controlling the kinetics of NO_3^- formation and yields during ozonation.

3.1.2. Nitrate yields of model amine compounds during ozonation

Amino acids. Eight amino acids with different side chains were studied, seven of which showed ≥90% conversion to nitrate ($[NO_3^-]$:$[amino\ acid]_0$) with a molar ratio $[O]_3$:$[amino\ acid]_0 = 20$ (Fig. 3). With one oxidant equivalent, an average NO_3^- yield of ≈14% was observed for 6 amino acids. This is only possible if some intermediate TPs are more reactive towards ozone than the precursors, because >1 molar equivalent of ozone is needed to transform an amine to nitrate. Exceptions were methionine and cysteine, containing an ozone-reactive sulfide or thiol group, respectively, which partially consume ozone via a fast reaction (von Sonntag and von Gunten, 2012). Since the sulfoxides are ozone-refractory, the sulfur reaction pathway of methionine is completed for 1 molar equivalent of ozone. Therefore, methionine showed a NO_3^- yield of 59.8% for a molar ratio $[O_3]$:$[methionine]_0 = 5$, which is similar to an average value of 53% for the other tested amino acids, excluding cysteine. A higher ozone demand for cysteine (requiring more than 1 molar equivalent of ozone for completion) was observed with NO_3^- yields of only 30.5% and 71.8%, for molar ratios $[O_3]$:$[amino\ acid]_0 = 5$ and 20, respectively.

Primary amines. NO_3^- yields of nine structurally different primary amines were determined (Fig. 3). In contrast to amino acids, great variability was observed among the tested compounds. BA, 4-chlorobenzylamine and 4-nitrobenzylamine showed the highest NO_3^- yields (>90% for $[O_3]$:$[amine]_0$ = 20). Ethanolamine, 2-phenylethylamine, *α*-methylamine and 3-phenyl-1-propylamine had intermediate yields (37–58%), while ethylamine and *β*-alanine had the lowest yields (<20%). Since ethylamine differed from L-alanine only by the absence of a carboxyl group on the *α*-carbon and *β*-alanine by a longer carbon

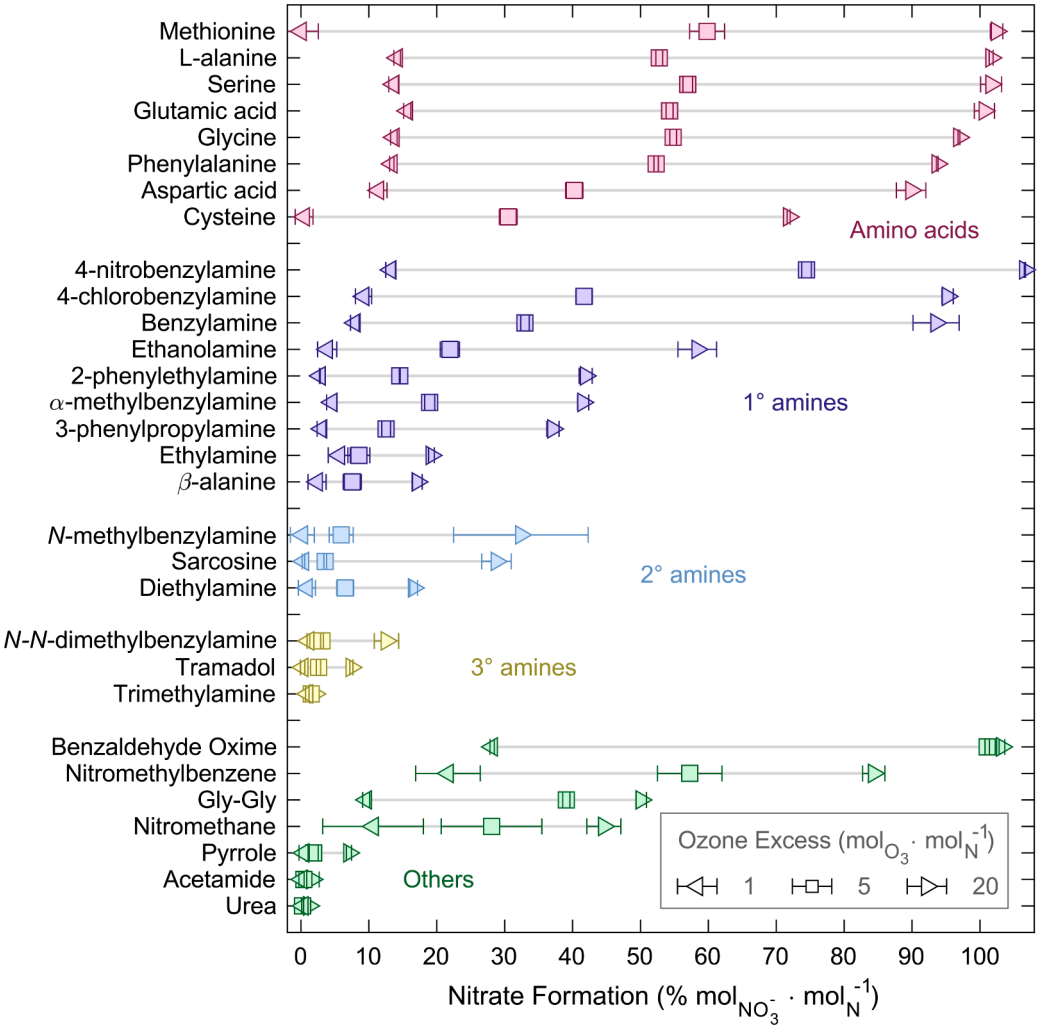

Fig. 3. Yields of nitrate from ozonation of model precursors for three specific ozone doses (1, 5 and 20 mol_{O3}/mol_N). Results reported as mean of triplicates (error bars depict standard deviations). Numerical values and chemical structures are provided in Table S5 (SI). Experimental conditions: $[precursor]_0 = 50$ µM, [*t*-BuOH] = 20 mM, pH 7.0 (phosphate buffer, $[PO_4^-]_{tot} = 5$ mM), t_{rx}=24 h, at room temperature (22±1°C). Potential residual ozone purged by N_2.

chain, it indicates that the carboxyl group in α-position to the amino group might play an important role.

Secondary amines. Secondary amines overall displayed a lower conversion to nitrate compared to primary amines (Fig. 3), which could be due to the greater degree of dealkylation required, which is not the main ozone reaction (Lim et al., 2019). Diethylamine (*N*-methylated ethylamine) formed 16.6% NO_3^- for a molar ratio $[O_3]$:$[amine]_0 = 20$, similar to ethylamine (19.2%). Under the same conditions, MBA (*N*-methylated benzylamine, 32.4%) and sarcosine (*N*-methylated glycine, 28.8%) displayed an augmented NO_3^- yield compared to diethylamine (16.6%). NO_3^- yields from secondary amines were equivocal and seemed to be structure dependent.

Tertiary amines. Three tertiary amines (*N-N*-dimethylbenzylamine, tramadol and trimethylamine) were ozonated, with all showing small NO_3^- yields, even at high specific ozone doses (Fig. 3).

Other N-containing functional groups. Due to the abundance of proteins and peptides in DON, the contribution of amides to nitrate formation was also explored. Two amide-containing compounds were tested - acetamide and diglycine (Gly-Gly). For acetamide, 2% yield of nitrate was obtained with a molar ratio $[O_3]$:$[acetamide]_0 = 20$. Gly-Gly contains 2 moles of N per molecule (peptide link and NH_2-terminus). At a molar ratio $[O_3]$:$[Gly\text{-}Gly]_0 = 20$, a NO_3^- yield of 50% was observed, suggesting that the terminal NH_2 group was fully converted to nitrate, with no significant contribution from the amide group. Further compounds which make up significant fractions of DON are urea and pyrrole. Urea, which contributes 0–65% (mean ± std: 6.9 ± 9.7% (mol/mol)) of the DON pool in natural estuarine environments and 6.4 ± 5.7% in riverine environments (Sipler and Bronk, 2015) formed almost no nitrate (Fig. 3). Pyrrole (abundant in waters due to its presence in chlorophyll, heme, porphyrins, histidine and tryptophan) (Tekle-Röttering et al., 2020), produced only 7% nitrate when oxidized with 20 molar equivalents of ozone.

3.1.3. *Transformation products formation and mechanistic considerations*

Our results suggest that the carbonyl group in α-position stimulates NO_3^- formation from amino acids during ozonation. Consistent NO_3^- yields for the tested amino acids indicate a similar ozone-oxidation pathway for all amino acids. The formation of nitrate from glycine has been previously studied (Berger et al., 1999; Lim et al., 2019; McCurry et al., 2016; Song et al., 2017; de Vera et al., 2017). Proposed mechanisms pass through several intermediates such as hydroxylamines, oximes or nitro(so)alkanes. Decarboxylation and hydrolysis were proposed as mechanisms forming nitrate. However, the mechanisms of NO_3^- formation from primary, secondary and tertiary amines during ozonation are still unclear, and the observed variability in NO_3^- formation was initially unexpected. To study these mechanisms in more detail, oxidation cascades of BA, MBA and DMBA were followed in batch dosages experiments.

BA yielded one of the highest NO_3^- yields among the selected primary amines. Fig. 4a shows the abatement of BA and the evolution of its TPs at pH 7, for specific ozone doses from 0 to 20 mol_{O3}/mol_N. The BA concentration decreased for molar ratios $[O_3]:[BA]_0$ <10 and was entirely abated at 10 molar equivalents of ozone. For molar ratios $[O_3]:[BA]_0 \leq 5$, the major TP was nitromethylbenzene (max. 76% of the abated BA), whereas NO_3^- also rose rapidly, already reaching 32% of the abated BA at a molar ratio $[O_3]:[BA] = 3$. Nitromethylbenzene was a transient TP, completely oxidized to NO_3^- with a yield of 91% at a molar ratio $[O_3]:[BA]_0 = 20$. This indirectly supports the amine oxide pathway (reactions (i), (j) and (g) in Fig. 4c) as the main oxidation mechanism. This pathway is also supported by sequentially increasing NO_3^- yields for benzylamine and nitromethylbenzene at molar ratios $[O_3]:[BA]_0$ of 1 and 5 (Fig. 3). Benzaldehyde oxime (nitromethylbenzene tautomer) was part of the analytical method, but not observed (reaction (k) in Fig. 4c).

The nitrogen mass balance was 89–103% for all ozone doses, which confirms that no major TPs were missed. Although not measured, NH_4^+ formation should consequently be minor, disqualifying the electron transfer pathway (reaction (h) in Fig. 4c). These results contrasted with a recent study showing that the only TP of ethylamine ozonation was nitroethane (tested molar ratios $[O_3]:[ethylamine]_0$: 0–3) and with a NO_3^- yield of only 10% for a 20-fold ozone excess (Lim et al., 2019). Another study also reported a complete transformation of methylamine to nitromethane at ≥12 molar equivalents of ozone (McCurry et al., 2016). Batch dosage experiments demonstrated that nitromethylbenzene forms more NO_3^- than nitromethane (Fig. 3), and we therefore hypothesize that electronic effects (induction, delocalization and resonance) play a decisive role in reactivity differences. The acid dissociation constant (K_a) is the most informative parameter related to electron withdrawing effects encountered by an amine group, as a

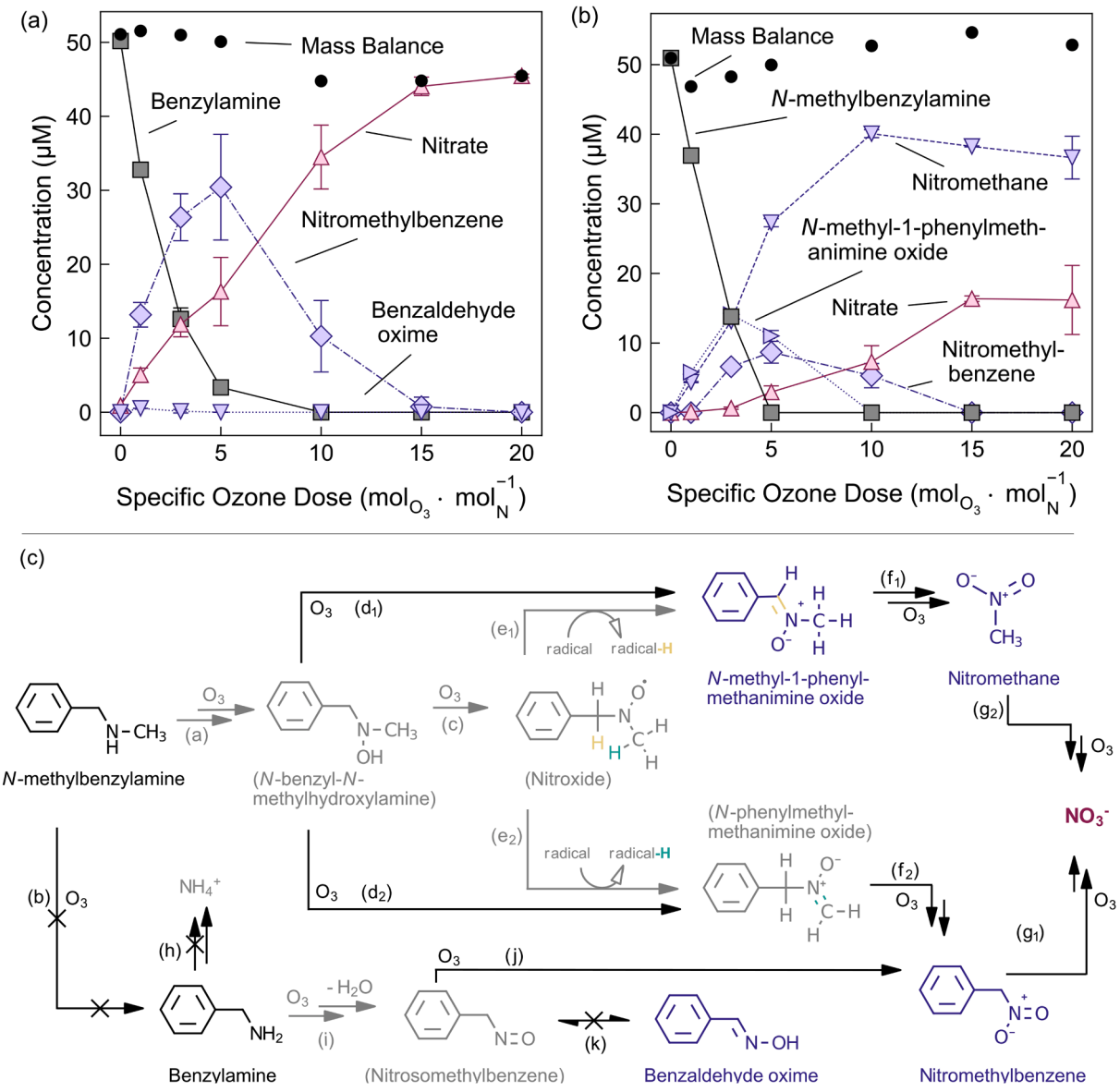

Fig. 4. Ozonation of (a) benzylamine (BA) and (b) *N*-methylbenzylamine (MBA) and the evolution of their transformation products as a function of the specific ozone dose (0 to 20 mol_{O3}/mol_N). Results reported as mean of triplicates (error bars depict standard deviations). Experimental conditions: $[benzylamine]_0 = [N\text{-methylbenzylamine}] = 50$ μM, [*t*-BuOH] = 20 mM, pH 7.0 (phosphate buffer, $[PO_4^-]_{tot} = 5$ mM), t_{rx}= 24 h, at room temperature (22±1°C). Potential residual ozone purged by N_2 after t_{rx}. (c) Possible reaction pathways for the ozonation of benzylamine and *N*-methylbenzylamine to nitrate, based on the results of this study ((a) and (b)) and proposed pathways in other studies, all cited in Text S8 (SI). Reactions (a)–(k) are described in detail in Text S8 (SI). Putative pathways and species are in gray; species in blue were measured in this study. "X" on an arrow means that the pathway was not observed. (For interpretation of the references to color in this figure legend, the reader is referred to the web version of this article.)

function of the chemical groups in its vicinity (Schwarzenbach et al., 2016). A strong positive correlation was observed between K_a and NO_3^- formation yields for 6 primary amines (Text S7, SI), supporting our hypothesis. The TP investigation for BA suggested that a C–N bond scission occurred after the formation of the nitro intermediate. Although not available, the α-carbon's pK_a should be influenced by the same factors as of the amine group. A lower pK_a could promote the formation of a carbanion, allowing an ozone attack on the α-carbon and resulting in a carbonyl-type compound, via an ozone-adduct. The latter could decompose, resulting in the corresponding aldehyde and NO_2^-, finally oxidized to NO_3^- by O_3. Our results suggest that the α-carbon's pK_a influences reaction (g) (Fig. 4c) to occur, in turn controlling the primary amine NO_3^- yields. This could possibly explain the observed heterogeneity in primary amine NO_3^- yields, which is supported by the key role of the α-carbon's pK_a already observed for the formation of nitromethane from several *N*-methylamines (reaction (d) in Fig. 4c) (Shi and McCurry, 2020).

MBA was entirely abated with a molar ratio $[O_3]:[MBA]_0 = 5$ (Fig. 4b). At a molar ratio $[O_3]:[MBA]_0=1$, *N*-methyl-1-phenylmethanimine oxide represented 42% of the abated MBA, and nitromethane 31%, with no contribution from nitrate or nitromethylbenzene. In the range $1<[O_3]:[MBA]_0\leq5$, three main TPs were gradually formed: *N*-methyl-1-phenylmethanimine oxide and nitromethane (in parallel), and nitromethylbenzene (with some delay, i.e., secondary TP). *N*-methyl-1-phenylmethanimine oxide and nitromethylbenzene were only transient TPs. *N*-methyl-1-phenylmethanimine oxide has been suggested as an intermediate between MBA and nitromethane (Shi and McCurry, 2020), which was corroborated in this study by its buildup in the range $1 \leq [O_3]:[MBA]_0 \leq 3$, followed by its abatement in the range $3 \leq [O_3]:[MBA]_0 \leq 10$. Nitromethane increased quantitatively with the abatement of *N*-methyl-1-phenylmethanimine oxide (Table S8, SI). At molar ratios $[O_3]:[MBA]_0 > 10$, nitromethane concentration reached a plateau, as *N*-methyl-1-phenylmethanimine oxide was depleted. After a concentration peak at a molar ratio of $[O_3]:[MBA]_0 = 5$, nitromethylbenzene was abated with an associated increase of the nitrate concentration (as observed for BA) and nitromethylbenzene was completely consumed at a molar ratio $[O_3]:[MBA]_0 = 15$. At a molar ratio $[O_3]:[MBA]_0 = 20$, the major final oxidation products were nitromethane (72%) and nitrate (32%), which complements recently published results on the ozonation of MBA (Shi and McCurry, 2020). No benzylamine was observed from the oxidation of MBA, disqualifying the electron transfer pathway for MBA too (reaction (b), Fig. 4c). The mass balance was 92–107% for all ozone doses, which confirms that no major TPs are missing. These observations suggest the occurrence of two oxidation pathways. From the initially formed hydroxylamine (reaction (a), Fig. 4c), two distinct imine oxides ($R_1C{=}N^+(-R_2)-O^-$ and $R_1N^+(=CR_2)-O^-$) could be formed by oxygen and/or electron transfer reactions (reactions (c), (d) and (e) in Fig. 4c). The transient imine oxides were further oxidized to the measured nitroalkanes, via two possible C–N bond cleavages (reaction (f), Fig. 4c). The final step is the nitroalkane oxidation to NO_3^-, for which the yield is structure-dependent, as discussed above and shown in Fig. 3 for nitromethane and nitromethylbenzene. In this case, nitromethane was favoured over nitromethylbenzene (for reasons discussed in Text S8, SI, reaction (f)) and the final NO_3^- yield was only 32.4%. Overall, this is in line with the previously proposed pathway for the reaction of diethylamine with ozone, for which, however, only one nitrone was observed because of the symmetry of the compound having 2 ethyl groups (Lim et al., 2019).

DMBA was quantitatively transformed to its *N*-oxide analogue with 1 molar ozone equivalent (Figure S4, SI). For higher ozone doses up to $[O_3]:[DMBA]_0 = 5$, only limited NO_3^- was formed (4%). This is in agreement with previous studies (Lim et al., 2019; Muñoz et al., 2001; Zimmermann et al., 2012). The mass balance was 100–106% for all ozone doses, which confirmed that no major TPs were missed.

3.1.4. NO_3^- formation potential as a proxy for N-DBP precursors

Based on these results, the NO_3^- formation potential can be regarded as an estimate of the highly reactive species in DON, mainly activated primary and secondary amines, and amino acids. Under realistic conditions (e.g., in a wastewater treatment plant), the formation of N-DBPs (i.e., intermediate compounds in the N oxidation cascade) can be formed, whereas in our continuous ozonation system, a large fraction of these specifically targeted intermediates (such as nitro or nitroso compounds) will be further oxidized to nitrate, depending on their reactivity and susceptibility (see Figs. 3 and 4). Therefore, nitrate formation during ozonation could be a potential proxy for the pool of reactive N-DBP precursors. Similar approaches exist to estimate other DBP precursor concentrations (Baird et al., 2017; Mitch and Sedlak, 2004), however, our approach may only cover part of the total pool of primary and secondary amines, even at high ozone doses. To overcome this potential underestimation, we assessed a complimentary second approach based on a FAC-titration.

3.2. Assessment of the chloramine formation with oxidative FAC-titrations

Chloramines are quickly formed by the reaction of chlorine with amines (Deborde and von Gunten, 2008). Therefore, one could indirectly quantify N-DBP precursors by quantifying chloramines with a non-selective method (DPD), after reaction with increasing doses of chlorine; this is the goal of the FAC-titrations. To this end, the oxidation conditions should maximize the formation of chloramines and minimize the consumption of chlorine by other reactive species. At pH 9.2, chlorine reacts fast with primary and secondary amines, as well as with activated phenolic compounds such as resorcinol (Fig. 1b). Optimal reaction times have to be chosen to satisfy the chlorine demand of amine model compounds or amine moieties in DOM, which was done by kinetic simulations of a simple reaction (amine + HOCl→ chloramine, with $k_{app,pH\ 9.2}$ defined in Text S9, SI), at several initial conditions.

3.2.1. Kinetic simulations and reaction time

Fig. 1d shows the modeled time for a 99% abatement ($t_{99\%}$) of 37 model amine compounds during chlorination ($[FAC]_0 = 15$ μM) at pH 9.2. For 36 amines, $t_{99\%}$ was smaller than 60 s. For diisopropylamine, a combination of high pK_a (11.07) and relatively low k_{HOCl} ($1.8{\cdot}10^7$ $M^{-1}s^{-1}$) leads to a longer $t_{99\%}$ of 139 s. Generally, secondary amines have lower k_{HOCl} than primary amines but similar pK_a-values, leading to higher $t_{99\%}$. Amino acids have intermediate pK_a-values (9.54–10.10) and high k_{HOCl} ($(0.32–1.13){\cdot}10^8$ $M^{-1}s^{-1}$), yielding low $t_{99\%}$. Finally, peptidic structures enhance the reactivity of the terminal amine by decreasing the pK_a (7.94–8.70), despite having k_{HOCl} values ($(0.6–1.26){\cdot}10^7$ $M^{-1}s^{-1}$) one order of magnitude lower than amino acids. Figure S5 (SI) compares the calculated $t_{99\%}$ of the 37 selected model amines for 6 FAC doses ranging between 10 and 40 μM, typically used in the oxidative FAC-titration experiments in this study. $[FAC]_0 = [amine]_0 = 10$ μM is the least favorable condition since 12 compounds (mostly secondary amines) had a $t_{99\%}>120$ s. With a $[FAC]_0 = 12$ μM, only diisopropylamine had a $t_{99\%}>120$ s and all amines had a $t_{99\%}<120$ s for a $[FAC]_0 = 20$ μM. Based on these observations, a reaction time (t_{rx}) of 120 s seemed reasonable for complex mixtures such as DOM. For the FAC-titrations of model compounds (glycine, methylamine and dimethylamine), a $t_{rx}=60$ s is sufficient, based on calculations with the same model

3.2.2. $(Boc)_2O$ derivatization efficiency

For primary and secondary amines, derivatization efficiencies were ≥97% (Figure S6, Table S9, SI). These results were comparable to already reported efficiencies (Einhorn et al., 1991; McCurry et al., 2016). In contrast, derivatization had no significant effect on the measured concentrations of either four phenolic compounds and *N*, *N*-dimethylbenzylamine, a tertiary amine (*p*-value >0.05) (Figure S11,

SI). This indicates that the derivatization procedure does not alter the nature of phenolic moieties but only transforms primary and secondary amines to carbamates. For benzylamine, the formation of *tert*-butyl-benzylcarbamate was qualitatively confirmed by retention time comparison (HPLC-UV) with a commercial standard (data not shown).

3.2.3. Oxidative FAC-titrations of model compounds

Fig. 5a–c and Table S9 (SI) show the results of oxidative FAC-titrations for three amine model compounds (glycine, methylamine and dimethylamine, $[amine]_0 = 10$ μM), as a function of the chlorine doses ($[FAC]_0 = 0–40$ μM) at pH 9.2. Residual FAC measurements resulted in two distinct phases. The initial phase (for FAC doses <10μM) was characterized by a full FAC consumption. The second phase showed a linear increase (for FAC doses >10 μM), with slopes of regression lines of about 1 (0.98–1.01) and intercepts close to 10 μM (9.10–10.91 μM), which corresponds to the initial amine concentration. In contrast, corresponding TC measurements were characterized by a single linear phase with slopes of about 1 (0.94–0.97) and intercepts not significantly different from zero (Table S9, SI). During the initial phase, the total applied FAC could be only measured as TC, meaning that the applied FAC was fully transformed to chloramine species. Thereafter, a constant difference (in μM) was observed between the parallel regression lines of TC and FAC (Fig. 5a–c). A 1:1 stoichiometric ratio can be considered for the reaction between FAC and amine moieties (Deborde and von Gunten, 2008). Therefore, the difference between the TC and FAC regression model intercepts (β_{FAC} and β_{TC}, respectively) corresponds to the initial total concentration of precursor amines:

$$\Delta\beta = \beta_{TC} - \beta_{FAC} = [\text{chloramines}]_{t=60s} = [\text{amines}]_{t=0s}$$

To confirm $\Delta\beta$ as a valid amine indicator, the same three model amines were FAC-titrated for the same conditions, but after $(BOC)_2O$-derivatization (Fig. 5d–f). In contrast to non-derivatized amines, no $\Delta\beta$ were observed (Table S9, SI), indicating that no chloramines were formed during chlorination. Identical slopes for FAC and TC close to 1 also confirmed that the added FAC remained unchanged in solution, in presence of carbamate.

Chlorine reactive phenolic compounds are present in DOM at much higher concentrations than nitrogen-containing species, therefore, their influence on oxidative FAC-titrations had to be tested. Phenol was selected as the simplest phenolic compound - its apparent second-order rate constant for the reaction with FAC under the conditions of the oxidative FAC-titrations at pH 9.2 ($k_{app,pH9.2}$= 78 $M^{-1}s^{-1}$ Deborde and von Gunten, 2008) is about 2'800 times lower than for glycine ($k_{app,pH9.2}$=2.2·10^5 $M^{-1}s^{-1}$ Deborde and von Gunten, 2008) (Fig. 1b). The oxidative FAC-titration of phenol resulted in slopes <1 for both regression lines (Figure S7a, SI). This indicates that phenol partially consumes the applied FAC dose, resulting, in this case, in a constant $[FAC]_{t=60\ s}/[FAC]_{t=0\ s}$ ratio of about 2/3, independent of $[FAC]_{t=0\ s}$. A kinetic simulation was performed, with the same conditions and based on known species-specific second-order rate constants for reaction of FAC with the phenolate ion and its chlorophenolate ions, which are formed upon chlorination (Table S10, SI). The kinetic simulation agreed well with the experimentally observed behavior of phenol during the oxidative FAC-titration (Figure S8, SI). In contrast, no FAC consumption was observed when 2,4,6-trimethylphenol was FAC-titrated since the three sites of possible FAC attack (in *ortho*- and *para*- positions) are blocked by methyl groups (Figure S7b, SI). Furthermore, experiments

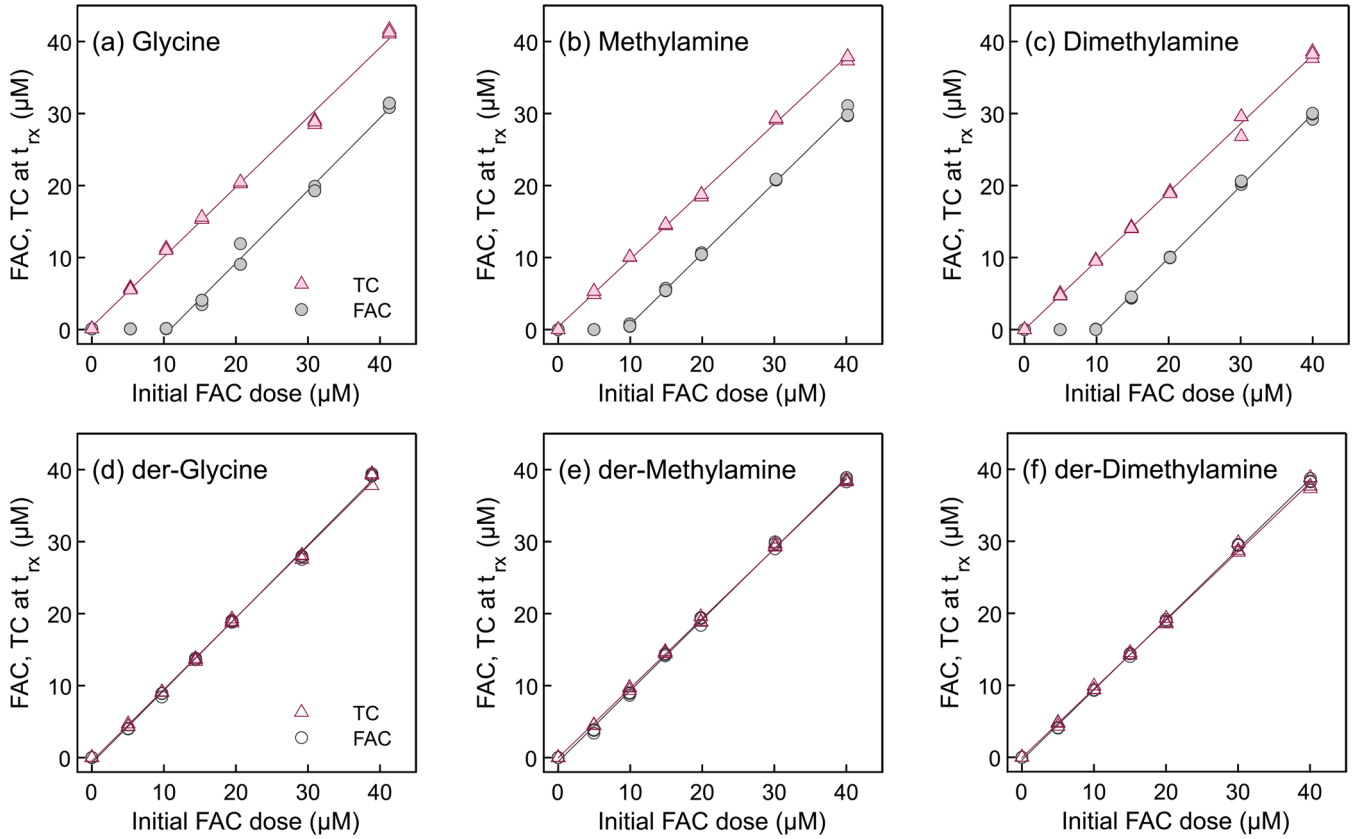

Fig. 5. Oxidative FAC-titrations for (a) glycine, (b) methylamine, (c) dimethylamine, and (d, e, f) their respective $(BOC)_2O$-derivatized forms ("der"). Circles are experimental results for free available chlorine (FAC) and triangles are experimental results for total chlorine (TC). Lines are linear regressions for each category of results (FAC or TC). Each data point represents a single independent experiment, with a given HOCl dose (at least 3 repetitions for each chlorine dose); all resulting points are shown (overlapping), without summary statistics. Table S9 (SI) compiles statistical analyses for the regression lines. Experimental conditions: $[amine]_0$ = 10 μM, $[FAC]_{t=0}$ ranged from 0 to 40 μM, pH 9.2 (carbonate buffer, $[CO_3^{2-}]_{tot}$=5 mM), t_{rx}=60 s, at room temperature (22±1°C).

were performed with resorcinol (benzene 1,3-diol, Figure S7c, SI), a phenolic compound with significantly higher chlorine-reactivity than phenol ($k_{app,pH9.2}$=2.0·10^4 M^{-1}s^{-1}) (Rebenne et al., 1996). A large initial phase of about 25 μM as well as a slope of about 2/3 were observed for a reaction time of 60 s, induced by both the rapid initial reaction of resorcinol with FAC and slower subsequent reactions between FAC and the ensuing products (Rebenne et al., 1996). An equivalent right shift should occur on the FAC and TC lines, having no influence on $\Delta\beta$, since no chloramines are formed from these compounds. Therefore, non-zero β_{TC} are an indication of the presence of rapidly reacting phenolic-type moieties.

Based on these results, $\Delta\beta$ is proposed as a novel reliable parameter, indirectly quantifying the total content of fast chlorine-reactive nitrogen compounds in aqueous solutions. This is a complementary indicator to the nitrate formation from ozonation discussed above.

3.3. Effects of controlled oxidative treatments on DOM properties

Four standard NOM/EfOM isolates (SRFA, SRNOM, UMRNOM & EfOM-CH) and two wastewater samples (WWTA and WWTB) were subjected to continuous ozonation and FAC-titration experiments. Changes in DOM bulk characteristics (nitrate and chloramine formation, and changes in optical properties) occurring as a function of ozone/chlorine treatment are discussed. Nitrate and chloramine formation were compared to the DON content of each water sample. WWTA and WWTB had a DON concentration of 1.30 ± 0.37 mg_N/L (93 ± 26 μM) and 1.14 ± 0.37 mg_N/L (80 ± 26 μM), respectively (Text S10, SI). Compared to NOM isolates, wastewater samples had higher specific DON concentrations (Fig. 6c). These values are in the range of typical DON concentration in wastewater effluents.

3.3.1. Nitrate formation

An optimal DON transformation to NO_3^- requires a large ozone excess, i.e., > 20 mol_{O3}/mol_N (Section 3.1.2). Practically, ozone exposures of about 0.32–0.57 M·s (256–456 mg min/L) could be reached in batch experiments containing only one ozone-reactive compound (Section 3.1.1). Further increasing the ozone exposures in such systems is impracticable due to the maximum ozone concentration of the ozone stock solution for our setup (i.e., ~1.1 mM). In DOM containing solutions, other faster reacting moieties (e.g., phenolic compounds, Fig. 1a) can act as competing ozone consumers (Önnby et al., 2018), lowering the ozone availability for nitrate formation. For these reasons, continuous ozonation experiments were developed in this study. In solutions containing DOM isolates or wastewater, the laboratory system (Fig. 2a) enabled high ozone exposures for a contact time of 120 min (i.e., 0.63–0.97 ·Ms or 504–776 mg min/L, Figure S9, SI). These are much higher than ozone exposures typically obtained in laboratory batch experiments with model water or wastewater effluents (Lee et al., 2014; Song et al., 2017; de Vera et al., 2017).

Upon continuous ozonation, a gradual NO_3^- production was observed for the four DOM isolates, but with different production rates (Fig. 6a). The NO_3^- production was biphasic, with a short initial phase with a high rate followed by a second longer phase with a lower rate (Figure S9, SI). The maximum NO_3^- formation potential was defined as the specific NO_3^- concentration resulting after a reaction time of 120 min and represented 13–20% of the total DON content (Fig. 6c). In the wastewater samples, the background NO_2^- also contributed to the formation of NO_3^- (Text S11, SI). To assess the NO_3^- formation potential of the DON matrix only, the total NO_3^- formation potential was corrected for the initial NO_2^- concentration (Fig. 6b). The corrected NO_3^- production curves were also

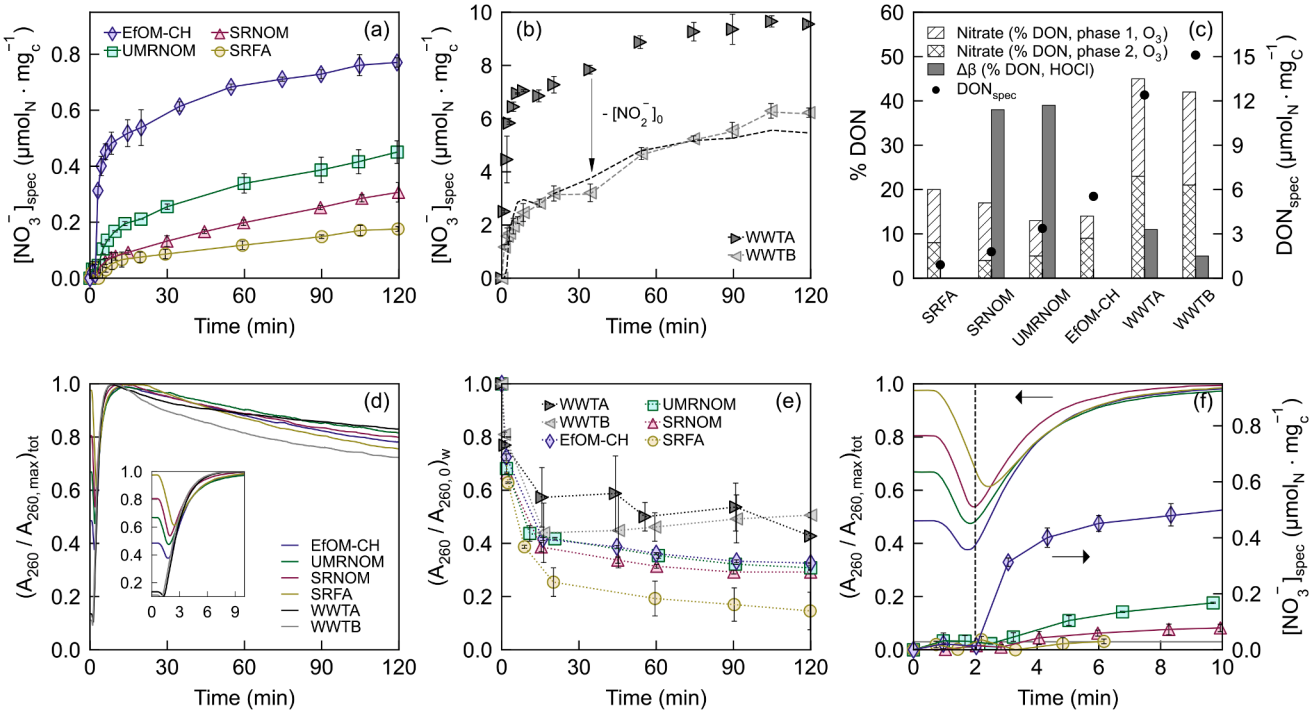

Fig. 6. Nitrate formation and relative change in absorbance at 260 nm for four isolates and two wastewater samples as a function of time, during continuous ozonation experiments. (a) Specific formation of NO_3^- for SRFA, SRNOM, UMRNOM and EfOM-CH (DOC_0 = 10 mg_C/L, spectrophotometrically standardized), (b) formation of NO_3^- for WWTA and WWTB (Table S4, SI), (c) nitrate formation (continuous ozonation) compared to the chloramine formation (FAC-titration), in percent of the specific DON content, (d) normalized absorbance at 260 nm of the whole solution (inserts: zoom on the initial phase), (e) change in water matrix absorbance at 260 nm relative to the initial DOM absorbance, (f) zoom on the 10 first minutes of the continuous ozonation experiments with the four NOM isolates showing the formation of NO_3^- together with the normalized absorbance at 260 nm of the whole solution (colors refer to the same isolates shown in (a) and (d)). Dashed lines in (d) are corrected NO_3^- concentrations (i.e., total NO_3^- - NO_3^- from initial NO_2^- oxidation (Text S11, SI)). Error bars depict the standard deviations of duplicate experiments and lines in (d) are averaged signals of duplicate experiments. Experimental conditions: pH 7.00±0.05 (phosphate buffer, $[PO_4^-]_{tot}$ = 10 mM), [*t*-BuOH] = 100 mM, continuous O_2/O gas bubbling during 120 min, at room temperature (22±1°C).

characterized by two phases (Figure S9, SI), separated by an intermediate plateau, and finally plateaued at about 42–45% of their DON content (Fig. 6c).

3.3.2. Effects of continuous ozonation on DOM optical properties

Fig. 6d shows the normalized absorbance of the solution at 260 nm ($(A_{260}/A_{260,max})_{tot}$) as a function of time, as monitored during continuous ozonation experiments. This indicator is influenced by two factors: (i) the water matrix absorbance ($A_{260,w}$) and (ii) the absorbance of dissolved ozone (A_{260,O_3}). During the initial phase ($t_{rx} < 4$ min), a V-shape evolution is visible (insert, Fig. 6d). Although a complete deconvolution of the signals is impossible (i.e., $A_{260,w}$ vs. A_{260,O_3}), it can be qualitatively interpreted: the descending branch is due to the initial decrease of DOM absorbance (between ~40 s and 120 s), whereas the ascending branch is attributed to the rapid ozone dissolution, reaching its maximum (i.e., $(A_{260}/A_{260,\,max})_{tot} = 1$) after about 10 min. The inflection point occurs at the moment where A_{260,O_3} outcompetes $A_{260,w}$. Overall, $(A_{260}/A_{260,max})_{tot}$ profiles are similar for all samples. The slowly decreasing phase observed after the maximum is due to the instability of the ozone generator, without having an influence on the experiments. Moreover, comparing $(A_{260}/A_{260,max})_{tot}$ at $t_{rx} = 0$ s between isolates renders information about their relative initial absorbance: SRFA > UMRNOM > SRNOM > EfOM-CH, in agreement with their $SUVA_{254}$ (Table S2, SI).

Fig. 6e shows the relative changes of absorbance at 260 nm of the water matrix ($(A_{260}/A_{260,0})_w$) as a function of time, during the same continuous ozonation experiments. This parameter decreased over time, i.e., with increasing ozone exposure. For the NOM isolates, a decrease of 30% occurred at the end of the initial descending branch (120 s) before plateauing at about 40% (25% for SRFA) of the initial $A_{260,w}$ at t_{rx}>10 min. For WWTA and WWTB, the initial decrease was smaller (about 20%) and the final plateau occurred at about 50% of the initial $A_{260,w}$ value.

3.3.3. Chloramine formation

Oxidative FAC-titrations of the four DOM isolates (DOC=5 mg_C/L) were carried out with a reaction time of 120 s. For SRNOM and UMRNOM (Fig. 7a, c), significant $\Delta\beta$ were observed (i.e., 0.68 and 1.32 $\mu mol_{HOCl}/mg_C$, respectively), indicating that 38–39% of their specific DON content formed chloramines upon oxidative FAC-titration (Fig. 6c). The same oxidative FAC-titrations performed after derivatization showed no significant $\Delta\beta$ (Figure S10, SI), confirming that $\Delta\beta$ consists of chlorine reactive nitrogen-containing compounds, which form chloramines. For SRFA (the fulvic acid fraction of SRNOM) and EfOM-CH (the hydrophobic fraction of the sampled EfOM), no significant $\Delta\beta$ were observed (Fig. 7b and d). A FAC slope of 0.80–0.84 (i.e., <1, Table S9, SI) for the four tested isolates revealed the presence of slower HOCl consuming compounds, which did not form chloramines. For wastewater samples, the background NH_3/NH_4^+ concentration also contributed to the formation of chloramines (Text S12, SI) (Wolfe et al., 1984). To assess the chloramine formation potential of the DON matrix only, the total chloramine formation potentials (Fig. 7e, f) were corrected for the initial NH_3/NH_4^+ concentrations. After correction, WWTA and WWTB showed significant $\Delta\beta$ of 1.31 (11% of the DON content) and 0.79 $\mu\mu mol_{HOCl}/mg_C$ (5%), respectively (Fig. 6c).

3.4. Characterization of DBP precursors and oxidation mechanisms in DOM

Fig. 6f compares $(A_{260}/A_{260,max})_{tot}$ and the specific NO_3^- formation for

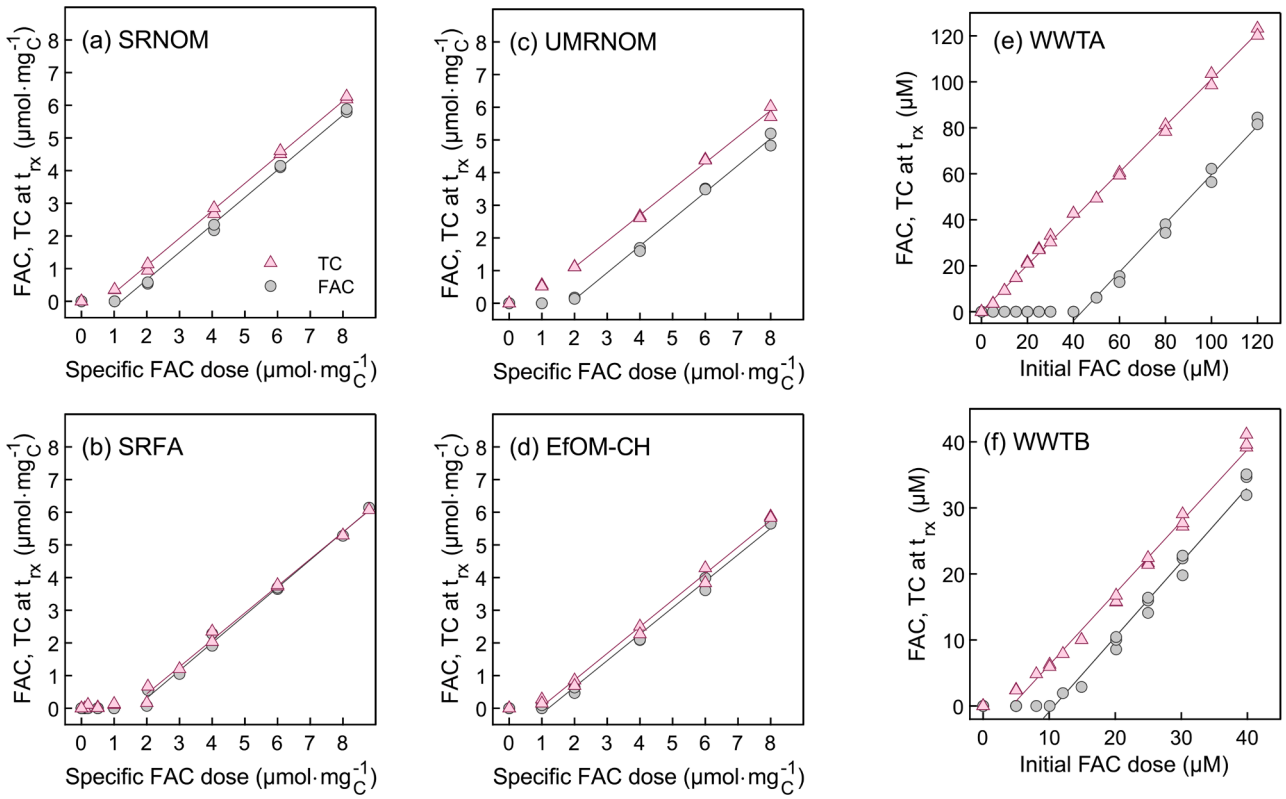

Fig. 7. Oxidative FAC-titrations of (a) SRNOM, (b) SRFA, (c) UMRNOM, (d) EfOM-CH, (e) WWTA, and (f) WWTB. Circles are experimental results for free available chlorine (FAC) and triangles are experimental results for total chlorine (TC). Lines are linear regressions for each category of results (FAC and TC). Each data point represents a single independent experiment, for a given FAC dose (at least 2 repetitions for each dose); all resulting points are shown (overlapping), without summary statistics. Table S9 (SI) compiles statistical analyses for the regression lines. Experimental conditions: DOC = 5.00 mg_C/L for NOM isolates ; 5.25 mg_C/L for WWTA ; 3.71 mg_C/L for WWTB, pH 9.2 (carbonate buffer, $[CO_3^{2-}]_{tot}$ = 5 mM), t_{rx}=120 s, at room temperature (22±1°C).

the 10 first minutes of the continuous ozonation experiments, for the four isolates. The NO_3^- formation started only after completion of the initial descending branch of $(A_{260}/A_{260,max})_{tot}$. Similarly, two steps could be observed during FAC-titrations of the four isolates: (i) a complete HOCl consumption at lower doses (i.e., significant β_{TC}, Table S9, SI) without formation of chloramines, and (ii) chloramines formation (i.e., significant $\Delta\beta$, Table S9, SI) and/or slow chlorine consumption (i.e., FAC and TC slopes <1, Table S9, SI) at higher doses (Fig. 7). These observations experimentally confirm a step-wise oxidation of electron-rich moieties in DOM, which has been hypothesized by kinetic modeling (Buffle et al., 2006). From a kinetic point of view, this corresponds to two main steps occurring successively: (i) oxidation of phenolic compounds; (ii) oxidation of amine compounds (Fig. 1a, b).

Decreases in $SUVA_{254}$ have been correlated with the abatement of conjugated NOM structures, by cleavage of aromatic rings (Remucal et al., 2020; von Sonntag and von Gunten, 2012; Weishaar et al., 2003; Wenk et al., 2013). Therefore, the observed initial changes in optical properties (i.e., initial descending $(A_{260}/A_{260,max})_{tot}$ branch and fast initial decrease in $(A_{260}/A_{260,0})_w$ are most likely caused by oxidation of phenolic moieties. Further decreases in $(A_{260}/A_{260,0})_w$ may be attributed to ring cleavages of other aromatic structures reacting more slowly with ozone, such as anisoles and polymethoxybenzenes, which are structures present in lignin (Mvula et al., 2009). By comparing the $(A_{260}/A_{260,max})_{tot}$ profile of each isolate and the profile of a control solution containing no DOM, the initial ozone exposure consumed by phenolic compounds (i.e., $t_{rx} \sim$ 40–120 s) could be calculated, from which the concentration of abated phenolic compounds was estimated (Text S13, SI). This results in 0.74–1.09 $\mu mol_{PhOH}/mg_C$ that were abated during this first phase, independently of the total phenolic content (Figure S11, SI). β_{TC} observed during FAC-titrations are in the same range (0.5–1.2 $\mu mol_{PhOH}/mg_C$, Figure S11, SI), suggesting that both assays also provide estimates for highly reactive phenolic compounds serving as DBP precursors, mainly resorcinol, hydroquinones and catechols, as previously observed (Arnold et al., 2008; Jiang et al., 2020; Zhao et al., 2012).

The formation of nitrate reveals the presence of mineralizable nitrogenous moieties, such as amino acids and activated primary and secondary amines (Section 3.1.2). The biphasic nature of the nitrate formation during ozonation suggests that various types of nitrogenous moieties were mineralized. The first phase was systematically associated with a higher $k_{f-NO_3^-}$ than the second phase (Figure S9, SI). According to the kinetic and dosage experiments with model compounds, the first phase may be attributed to compounds forming nitrate quickly (i.e., amino acids, phase 1 in Fig. 6c) with estimated second-order rate constants $k_{f-NO_3^-}$ in the range of 2.5–6.5 $M^{-1}s^{-1}$, which is similar to L-alanine (7.1 $M^{-1}s^{-1}$). For instance, the estimated content of fast reacting amine moieties in SRFA was 0.07 $\mu mol_N/mg_C$, which corroborates well with a previously reported amino acid concentration (0.08 $\mu mol_N/mg_C$) (Averett et al., 1994). For all isolates, the first phase represented less than 10% of their total DON content, which is lower than for WWTA and WWTB (25%, Fig. 6c). The second phase may be attributed to mineralizable primary and secondary amines (phase 2, Fig. 6c) with $k_{f-NO_3^-}$ in the range of 0.1–0.3 $M^{-1}s^{-1}$, which is closer to β-alanine (0.1 $M^{-1}s^{-1}$) or *N*-methylbenzylamine (0.6 $M^{-1}s^{-1}$). Comparatively, the total content of amino-acids and primary and secondary amines is quantified during FAC-titrations. For SRNOM and UMRNOM, the chloramine formation (40% of DON, Fig. 6c) was higher than the nitrate formation (25% of DON) and the difference may be attributed to the fraction of primary and secondary amines which is not easily mineralized. Nevertheless, this difference is still within a factor of two, which is a reasonable overlap considering the different nature of the two assays. Although these moieties are not forming nitrate quantitatively (i.e., not quantified by continuous ozonation), they can still form N-DBPs such as nitroalkanes upon ozonation, as was demonstrated in this study and in previous investigations (Lim et al., 2019). For SRFA and EfOM-CH, a low nitrate formation was observed (i.e., ≤20% of DON) together with an absence of measurable chloramine formation (Fig. 6c). For SRFA, the absence of measurable $\Delta\beta$ may be due to a too high LOQ for the FAC-titration method (0.5 $\mu mol_N/mg_C$) which is higher than the formation of nitrate measured during ozonation (0.19 $\mu mol_N/mg_C$). The kinetics of NO_3^- formation for EfOM-CH were higher than for the other isolates (Fig. 6a), but closer to the WWTA/B samples. This suggests that other compounds could be responsible for it, such as partially oxidized biomolecules produced during biological wastewater treatment.

WWTA and WWTB had low chloramine formation yields (5–11%) and high NO_3^- yields (42–45%). The initial nitrate formation kinetics is extremely high with $k_{f-NO_3^-}$ in the range of 23–29 $M^{-1}s^{-1}$. These values are far above the $k_{f-NO_3^-}$ for the probe compounds and suggest a direct formation from intermediate compounds. The second phase is then again comparable to β-alanine and *N*-methylbenzylamine. This suggests that 34–37% of their DON is composed of moieties which are ozone-reactive but not forming chloramines during chlorination. They are therefore not amino acids or amines, but could be partially oxidized nitrogenous compounds or other biomolecules formed during nitrification, where N–O-containing compounds could be formed. As a consequence, the corresponding nitrogen-containing moieties are not readily available for chlorination. Although being significant contributors to the N-DBP formation potentials, the exact nature of these species remains unknown. Nevertheless, the behavior is in agreement with, e.g., 4-nitrobenzylamine, which was efficiently transformed to nitrate upon ozonation.

Overall, the novel approaches applied in this study show that ozone and FAC-titrations provide complimentary information for the characterization of DOM in terms of potential N-DBP precursors quantification and characterization. In the tested samples, up to 40% of the DON is chlorine and/or ozone reactive and serves as N-DBP precursors. Furthermore, there was a reasonable agreement between ozone and FAC-titrations regarding the fast reactive moieties in NOM samples, which may lead to C-DBPs. Finally, our findings reveal clear differences between the selected NOM/EfOM isolates and the real water samples, however, no general conclusions can be drawn.

3.5. Practical implications

Previous laboratory-scale studies mostly focused on the yields of N-DBP formation from specific model compounds or standard NOM sources under excess oxidant conditions, which could lead to DBP overestimation under real oxidation conditions (Bond et al., 2012). In the proposed approach, a subtle change of perspective is proposed, by focusing on the specific quantification of common oxidation products (nitrate and chloramines) formed upon controlled oxidation experiments with ozone or chlorine. Nitrate is the end product of the nitrogen oxidation cascade and our study demonstrates that intermediate N-DBPs are formed at lower ozone doses. In that sense, the nitrate formation is an unambiguous indicator of the N-DBP formation potential, because nitrate is formed only after extensive ozonation via intermediate TPs. This suggests that the fraction of DON that can form undetected N-DBPs during ozonation is high. In WWTP including an ozonation step, moderate ozone doses are typically targeted (0.55–0.65 g_{O3}/g_{DOC}) (Bourgin et al., 2018). It can be assumed, that phenolic moieties consumed 0.02–0.21 g_{O3}/g_{DOC} during the initial phase of continuous ozonation experiments (Text S13, SI). Therefore, a significant part of the applied ozone dose could subsequently oxidize DON, forming various N-DBPs, even under realistic ozonation conditions. FAC-titrations offer complimentary information about the nature of the N-DBP precursors, as not all primary and secondary amines form nitrate readily upon ozonation. This permits to estimate the concentration of N-DBP precursors present in a water sample, also including primary and secondary amines which are only partially oxidized to e.g., nitroalkanes during ozonation.

4. Conclusion

In this study, kinetics and mechanisms of NO_3^- formation by the reaction of amine compounds with ozone have been studied with model compounds, DOM isolates and wastewater samples. Moreover, a combination of two novel oxidation assays was developed and applied to better characterize the nature of oxidant-reactive nitrogenous moieties in DOM. The following conclusions can be drawn:

- Molar NO_3^- yields of 30 nitrogenous model compounds have been determined in ozone dosage experiments, at pH 7. With 20 molar equivalents of ozone, amino acids and activated primary amines showed the highest yields (>90%), followed by other primary and secondary amines (20–50%) and tertiary amines (<15%). This information can serve as a basis for a better understanding of reactivity of nitrogenous moieties in DOM.
- Nitroalkanes are major intermediate TPs in the oxidation cascade of primary and secondary amines, e.g., nitromethylbenzene (benzylamine and *N*-methylbenzylamine) and nitromethane (*N*- methylbenzylamine). For secondary amines, the formation of nitroalkane occurs by C=N bond cleavage on nitrone intermediates, e.g., *N*-methyl-1-phenylmethanimine oxide and *N*-phenylmethylmethanimine oxide (*N*- methylbenzylamine).
- The nitrate formation potential of a nitrogenous compound is not correlated to its apparent second-order rate constant for the reaction with ozone, but it is related to its chemical structure. In particular, the presence of an electron-withdrawing group in the vicinity of the amine group promotes the formation of NO_3^- by decreasing the pK_a-value of the α-carbon on intermediate nitroalkanes.
- The formation of NO_3^- in NOM/EfOM and wastewater samples during continuous ozonation is biphasic. The first phase is attributed to amino acids and the second phase to mineralizable primary and secondary amines, as kinetically determined. This is an effective way to characterize and quantify the DON fraction which is ozone-reactive. This fraction was higher for wastewater samples than for NOM/EfOM isolates (i.e., 40% vs. <20%). For wastewater samples, the formation of NO_3^- was also faster.
- FAC-titration is a complementary method used to reveal the formation of chloramines in NOM/EfOM or wastewater samples, as a proxy for the total primary and secondary amine content.
- For two NOM isolates (SRNOM and UMRNOM), the DON fraction which is chlorine-reactive was higher than the DON fraction which is ozone reactive (i.e., 40% vs. <20%). This reveals the presence of primary and secondary amines which are not forming NO_3^- quantitatively but that can potentially form nitroalkanes. In contrast, wastewater samples had higher ozone-reactive DON fractions than chlorine-reactive fractions (i.e., 40% vs. ≤11%), revealing the presence of partially oxidized nitrogenous compounds with a N-O bond, formed during nitrification. These observations highlight the good complementarity of both assays in deconvoluting the composition of the DON pool.
- Oxidant-reactive phenolic compound concentrations could also be estimated by both methods and were in the range 0.5–1.2 $\mu mol_{PhOH}/mg_C$ for the NOM/EfOM isolates.
- Overall, the tested samples had a significant oxidant-reactive DON fraction (up to 45%) which could lead to the formation of μM-levels of potentially toxic N-DBPs such as nitro-compounds during ozonation of drinking water or wastewater. The presented assays can help to gauge this level for specific water samples. A post-chlorination could potentially lead to the formation of toxic halonitro-compounds.

Declaration of Competing Interest

The authors declare that they have no known competing financial interests or personal relationships that could have appeared to influence the work reported in this paper.

Acknowledgments

We thank Caroline Gachet-Acquillon for her support in the laboratory and with chromatographic techniques, Natalie Gsteiger and her team (AuA lab, Eawag, Dübendorf, Switzerland) for the measurements of basic wastewater parameters, Jacqueline Traber for the SEC-UV-OCD-ND measurements (Eawag), Dominique Grandjean for his support with GC–MS/MS measurements, Eva Rodriguez for interesting discussions and inputs, as well as Ingo Schoppe and Adrian Baumann for providing samples from the WWTP Thunersee and their interest in participating in the project. We also thank the Swiss National Science Foundation (SNSF) for financial support (project no. 200021-181975).

Supplementary material

Supplementary material associated with this article can be found, in the online version, at doi:10.1016/j.watres.2021.117864

References

Aieta, E.M., Roberts, P.V., Hernandez, M., 1984. Determination of chlorine dioxide, chlorine, chlorite, and chlorate in water. J. Am. Water Works Assoc. 76 (1), 64–70.

Arnold, W.A., Bolotin, J., von Gunten, U., Hofstetter, T.B., 2008. Evaluation of functional groups responsible for chloroform formation during water chlorination using compound specific isotope analysis. Environ. Sci. Technol. 42 (21), 7778–7785. https://doi.org/10.1021/es800399a.

Averett, R. C., Leenheer, J. A., McKnight, D. M., Thorn, K., 1994. Humic substances in the Suwannee River, Georgia; interactions, properties, and proposed structures. 10.3133/wsp2373.

Bader, H., Hoigné, J., 1981. Determination of ozone in water by the indigo method. Water Res. 15 (4), 449–456. https://doi.org/10.1016/0043-1354(81)90054-3.

Bader, H., Sturzenegger, V., Hoigné, J., 1988. Photometric method for the determination of low concentrations of hydrogen peroxide by the peroxidase catalyzed oxidation of *N,N*-diethyl-*p*-phenylenediamine (DPD). Water Res. 22 (9), 1109–1115. https://doi.org/10.1016/0043-1354(88)90005-X.

Baird, R., Eaton, A.D., Rice, E.W., Bridgewater, L, American Public Health Association, American Water Works Association, Water Environment Federation, 2017. Standard Methods for the Examination of Water and Wastewater. American Public Health Association.

Berger, P., Karpel Vel Leitner, N., Doré, M., Legube, B., 1999. Ozone and hydroxyl radicals induced oxidation of glycine. Water Res. 33 (2), 433–441. https://doi.org/10.1016/S0043-1354(98)00230-9.

Bond, T., Templeton, M.R., Graham, N., 2012. Precursors of nitrogenous disinfection by-products in drinking water—A critical review and analysis. J. Hazard. Mater. 235–236, 1–16. https://doi.org/10.1016/j.jhazmat.2012.07.017.

Bourgin, M., Beck, B., Boehler, M., Borowska, E., Fleiner, J., Salhi, E., Teichler, R., von Gunten, U., Siegrist, H., McArdell, C.S., 2018. Evaluation of a full-scale wastewater treatment plant upgraded with ozonation and biological post-treatments: abatement of micropollutants, formation of transformation products and oxidation by-products. Water Res. 129, 486–498. https://doi.org/10.1016/j.watres.2017.10.036.

Buffle, M.-O., Schumacher, J., Salhi, E., Jekel, M., von Gunten, U., 2006. Measurement of the initial phase of ozone decomposition in water and wastewater by means of a continuous quench-flow system: application to disinfection and pharmaceutical oxidation. Water Res. 40 (9), 1884–1894. https://doi.org/10.1016/j.watres.2006.02.026.

Chon, K., Lee, Y., Traber, J., von Gunten, U., 2013. Quantification and characterization of dissolved organic nitrogen in wastewater effluents by electrodialysis treatment followed by size-exclusion chromatography with nitrogen detection. Water Res. 47 (14), 5381–5391. https://doi.org/10.1016/j.watres.2013.06.019.

Council, N.R., 2012. Water Reuse: Potential for Expanding the Nation's Water Supply Through Reuse of Municipal Wastewater. Technical Report. National Academies Press, Washington, D.C. https://doi.org/10.17226/13303

Deborde, M., von Gunten, U., 2008. Reactions of chlorine with inorganic and organic compounds during water treatment—Kinetics and mechanisms: acritical review. Water Res. 42 (1–2), 13–51. https://doi.org/10.1016/j.watres.2007.07.025.

Delpla, I., Jung, A.-V., Baures, E., Clement, M., Thomas, O., 2009. Impacts of climate change on surface water quality in relation to drinking water production. Environ. Int. 35 (8), 1225–1233. https://doi.org/10.1016/j.envint.2009.07.001.

Dotson, A., Westerhoff, P., 2009. Occurrence and removal of amino acids during drinking water treatment. J. Am. Water Works Assoc. 101 (9), 101–115. https://doi.org/10.1002/j.1551-8833.2009.tb09963.x.

Einhorn, J., Einhorn, C., Luche, J.-L., 1991. A mild and efficient sonochemical tert-butoxycarbonylation of amines from their salts. Synlett 1991 (1), 37–38. https://doi.org/10.1055/s-1991-20620.

Gerrity, D., Pecson, B., Trussell, R.S., Trussell, R.R., 2013. Potable reuse treatment trains throughout the world. J. Water Supply 62 (6), 321–338. https://doi.org/10.2166/aqua.2013.041.

Graeber, D., Boëchat, I.G., Encina-Montoya, F., Esse, C., Gelbrecht, J., Goyenola, G., Gücker, B., Heinz, M., Kronvang, B., Meerhoff, M., Nimptsch, J., Pusch, M.T., Silva, R.C.S., von Schiller, D., Zwirnmann, E., 2015. Global effects of agriculture on fluvial dissolved organic matter. Sci. Rep. 5 (1), 1–8. https://doi.org/10.1038/srep16328.

von Gunten, U., 2018. Oxidation processes in water treatment: are we on track? Environ. Sci. Technol. 52 (9), 5062–5075. https://doi.org/10.1021/acs.est.8b00586.

von Gunten, U., Salhi, E., Schmidt, C.K., Arnold, W.A., 2010. Kinetics and mechanisms of *N*-nitrosodimethylamine formation upon ozonation of n, n -dimethylsulfamide-containing waters: bromide catalysis. Environ. Sci. Technol. 44 (15), 5762–5768. https://doi.org/10.1021/es1011862.

Hand, V.C., Margerum, D.W., 1983. Kinetics and mechanisms of the decomposition of dichloramine in aqueous solution. Inorg. Chem. 22 (10), 1449–1456. https://doi.org/10.1021/ic00152a007.

Heeb, M.B., Kristiana, I., Trogolo, D., Arey, J.S., von Gunten, U., 2017. Formation and reactivity of inorganic and organic chloramines and bromamines during oxidative water treatment. Water Res. 110, 91–101. https://doi.org/10.1016/j.watres.2016.11.065.

Hoigné, J., Bader, H., 1994. Kinetics of reactions of chlorine dioxide (OClO) in water-I. Rate constants for inorganic and organic compounds. Water Res. 28 (1), 45–55. https://doi.org/10.1016/0043-1354(94)90118-X.

Jiang, J., Han, J., Zhang, X., 2020. Nonhalogenated aromatic DBPs in drinking water chlorination: a gap between NOM and halogenated aromatic DBPs. Environ. Sci. Technol. 54 (3), 1646–1656. https://doi.org/10.1021/acs.est.9b06403.

Jørgensen, N.O.G., 2009. Organic nitrogen. In: Likens, G.E. (Ed.), Encyclopedia of Inland Waters. Academic Press, Oxford, pp. 832–851. https://doi.org/10.1016/B978-012370626-3.00119-8.

Jørgensen, N.O.G., Stepanaukas, R., Pedersen, A.-G.U., Hansen, M., Nybroe, O., 2003. Occurrence and degradation of peptidoglycan in aquatic environments. FEMS Microbiol. Ecol. 46 (3), 269–280. https://doi.org/10.1016/S0168-6496(03)00194-6.

Krasner, S.W., 2009. The formation and control of emerging disinfection by-products of health concern. Philos. Trans. R. Soc. A 367 (1904), 4077–4095. https://doi.org/10.1098/rsta.2009.0108.

Krasner, S.W., Weinberg, H.S., Richardson, S.D., Pastor, S.J., Chinn, R., Sclimenti, M.J., Onstad, G.D., Thruston, A.D., et al., 2006. Occurrence of a new generation of disinfection byproducts. Environ. Sci. Technol. 40 (23), 7175–7185. https://doi.org/10.1021/es060353j.

Lee, Y., Kovalova, L., McArdell, C.S., von Gunten, U., 2014. Prediction of micropollutant elimination during ozonation of a hospital wastewater effluent. Water Res. 64, 134–148. https://doi.org/10.1016/j.watres.2014.06.027.

Leenheer, J.A., Croué, J.-P., 2003. Characterizing aquatic dissolved organic matter. Environ. Sci. Technol. 37 (1), 18A–26A. https://doi.org/10.1021/es032333c.

Li, X.-F., Mitch, W.A., 2018. Drinking water disinfection byproducts (DBPs) and human health effects: multidisciplinary challenges and opportunities. Environ. Sci. Technol. 52 (4), 1681–1689. https://doi.org/10.1021/acs.est.7b05440.

Lim, S., McArdell, C.S., von Gunten, U., 2019. Reactions of aliphatic amines with ozone: kinetics and mechanisms. Water Res. 157, 514–528. https://doi.org/10.1016/j.watres.2019.03.089.

Liu, H., Jeong, J., Gray, H., Smith, S., Sedlak, D.L., 2012. Algal uptake of hydrophobic and hydrophilic dissolved organic nitrogen in effluent from biological nutrient removal municipal wastewater treatment systems. Environ. Sci. Technol. 46 (2), 713–721. https://doi.org/10.1021/es203085y.

Marron, E.L., Mitch, W.A., von Gunten, U., Sedlak, D.L., 2019. A tale of two treatments: the multiple barrier approach to removing chemical contaminants during potable water reuse. Acc. Chem. Res. 52 (3), 615–622. https://doi.org/10.1021/acs.accounts.8b00612.

McCurry, D.L., Quay, A.N., Mitch, W.A., 2016. Ozone promotes chloropicrin formation by oxidizing amines to nitro compounds. Environ. Sci. Technol. 50 (3), 1209–1217. https://doi.org/10.1021/acs.est.5b04282.

Mitch, W.A., Sedlak, D.L., 2002. Formation of *N*-nitrosodimethylamine (NDMA) from dimethylamine during chlorination. Environ. Sci. Technol. 36 (4), 588–595. https://doi.org/10.1021/es010684q.

Mitch, W.A., Sedlak, D.L., 2004. Characterization and fate of *N*-nitrosodimethylamine precursors in municipal wastewater treatment plants. Environ. Sci. Technol. 38 (5), 1445–1454. https://doi.org/10.1021/es035025n.

Muñoz, F., Mvula, E., Braslavsky, S.E., von Sonntag, C., 2001. Singlet dioxygen formation in ozone reactions in aqueous solution. J. Chem. Soc., Perkin Trans. 2 0 (7), 1109–1116. https://doi.org/10.1039/b101230o.

Muñoz, F., von Sonntag, C., 2000. The reactions of ozone with tertiary amines including the complexing agents nitrilotriacetic acid (NTA) and ethylenediaminetetraacetic acid (EDTA) in aqueous solution. J. Chem. Soc., Perkin Trans. 2 (10), 2029–2033. https://doi.org/10.1039/b004417m.

Muellner, M.G., Wagner, E.D., McCalla, K., Richardson, S.D., Woo, Y.-T., Plewa, M.J., 2007. Haloacetonitriles vs. regulated haloacetic acids: are nitrogen-containing DBPs more toxic? Environ. Sci. Technol. 41 (2), 645–651. https://doi.org/10.1021/es0617441.

Mvula, E., Naumov, S., von Sonntag, C., 2009. Ozonolysis of lignin models in aqueous solution: anisole, 1,2-dimethoxybenzene, 1,4-dimethoxybenzene, and 1,3,5-trimethoxybenzene. Environ. Sci. Technol. 43 (16), 6275–6282. https://doi.org/10.1021/es900803p.

Önnby, L., Walpen, N., Salhi, E., Sander, M., von Gunten, U., 2018. Two analytical approaches quantifying the electron donating capacities of dissolved organic matter to monitor its oxidation during chlorination and ozonation. Water Res. 144, 677–689. https://doi.org/10.1016/J.WATRES.2018.06.060.

Parkin, G.F., McCarty, P.L., 1981. A comparison of the characteristics of soluble organic nitrogen in untreated and activated sludge treated wastewaters. Water Res. 15 (1), 139–149. https://doi.org/10.1016/0043-1354(81)90194-9.

Pehlivanoglu-Mantas, E., Sedlak, D.L., 2006. Wastewater-derived dissolved organic nitrogen: analytical methods, characterization, and effects—areview. Crit. Rev. Environ. Sci. Technol. 36 (3), 261–285. https://doi.org/10.1080/10643380500542780.

Pehlivanoglu-Mantas, E., Sedlak, D.L., 2008. Measurement of dissolved organic nitrogen forms in wastewater effluents: concentrations, size distribution and NDMA formation potential. Water Res. 42 (14), 3890–3898. https://doi.org/10.1016/j.watres.2008.05.017.

Pinkernell, U., Nowack, B., Gallard, H., von Gunten, U., 2000. Methods for the photometric determination of reactive bromine and chlorine species with ABTS. Water Res. 34 (18), 4343–4350. https://doi.org/10.1016/S0043-1354(00)00216-5.

Plewa, M.J., Wagner, E.D., Jazwierska, P., Richardson, S.D., Chen, P.H., McKague, A.B., 2004. Halonitromethane drinking water disinfection byproducts: chemical characterization and mammalian cell cytotoxicity and genotoxicity. Environ. Sci. Technol. 38 (1), 62–68. https://doi.org/10.1021/es030477l.

Rebenne, L.M., Gonzalez, A.C., Olson, T.M., 1996. Aqueous chlorination kinetics and mechanism of substituted dihydroxybenzenes. Environ. Sci. Technol. 30 (7), 2235–2242. https://doi.org/10.1021/es950607t.

Remucal, C.K., Salhi, E., Walpen, N., von Gunten, U., 2020. Molecular-level transformation of dissolved organic matter during oxidation by ozone and hydroxyl radical. Environ. Sci. Technol. 54 (16), 10351–10360. https://doi.org/10.1021/acs.est.0c03052.

Richardson, S.D., Plewa, M.J., Wagner, E.D., Schoeny, R., DeMarini, D.M., 2007. Occurrence, genotoxicity, and carcinogenicity of regulated and emerging disinfection by-products in drinking water: a review and roadmap for research. Mutat. Res./Rev. Mutat. Res. 636 (1), 178–242. https://doi.org/10.1016/j.mrrev.2007.09.001.

Rodier, J., Legube, B., Merlet, N., 2016. L'analyse de l'Eau, tenth ed. Dunod.

Rosario-Ortiz, F., Rose, J., Speight, V., Von Gunten, U., Schnoor, J., 2016. How do you like your tap water? Science 351 (6276), 912–914.

Schwarzenbach, R.P., Gschwend, P.M., Imboden, D.M., 2016. Environmental Organic Chemistry. John Wiley & Sons.

Sedlak, D., 2014. Water 4.0: The Past, Present, and Future of the World's Most Vital Resource.

Shi, J.L., McCurry, D.L., 2020. Transformation of *N*-methylamine drugs during wastewater ozonation: formation of nitromethane, an efficient precursor to halonitromethanes. Environ. Sci. Technol. 54 (4), 2182–2191. https://doi.org/10.1021/acs.est.9b04742.

Shon, H.K., Vigneswaran, S., Snyder, S.A., 2006. Effluent organic matter (EfOM) in wastewater: constituents, effects, and treatment. Crit. Rev. Environ. Sci. Technol. 36 (4), 327–374. https://doi.org/10.1080/10643380600580011.

Sipler, R.E., Bronk, D.A., 2015. Chapter 4 - dynamics of dissolved organic nitrogen. In: Hansell, D.A., Carlson, C.A. (Eds.), Biogeochemistry of Marine Dissolved Organic Matter, second ed. Academic Press, Boston, pp. 127–232. https://doi.org/10.1016/B978-0-12-405940-5.00004-2.

Song, Y., Breider, F., Ma, J., von Gunten, U., 2017. Nitrate formation during ozonation as a surrogate parameter for abatement of micropollutants and the n-nitrosodimethylamine (NDMA) formation potential. Water Res. 122, 246–257. https://doi.org/10.1016/j.watres.2017.05.074.

Stalter, D., O'Malley, E., von Gunten, U., Escher, B.I., 2016. Fingerprinting the reactive toxicity pathways of 50 drinking water disinfection by-products. Water Res. 91, 19–30. https://doi.org/10.1016/J.WATRES.2015.12.047.

Tekle-Röttering, A., Lim, S., Reisz, E., Holger, V.L., Sajjad Abdighahroudi, M., Willach, S., Schmidt, W., Peter, R.T., Rentsch, D., Christa, S.M., Torsten, C.S., von Gunten, U., 2020. Reactions of pyrrole, imidazole, and pyrazole with ozone: kinetics and mechanisms. Environ. Sci. 6 (4), 976–992. https://doi.org/10.1039/C9EW01078E.

de Vera, G.A., Gernjak, W., Weinberg, H., Farré, M.J., Keller, J., von Gunten, U., 2017. Kinetics and mechanisms of nitrate and ammonium formation during ozonation of dissolved organic nitrogen. Water Res. 108, 451–461. https://doi.org/10.1016/j.watres.2016.10.021.

von Sonntag, C., von Gunten, U., 2012. Chemistry of Ozone in Water and Wastewater Treatment-From Basic Principles to Applications. IWA Publishing.

Wagner, E.D., Plewa, M.J., 2017. CHO cell cytotoxicity and genotoxicity analyses of disinfection by-products: an updated review. J. Environ. Sci. 58, 64–76. https://doi.org/10.1016/j.jes.2017.04.021.

Wajon, J.E., Morris, J.C., 1982. Rates of formation of N-bromo amines in aqueous solution. Inorg. Chem. 21 (12), 4258–4263. https://doi.org/10.1021/ic00142a030.

Weishaar, J.L., Aiken, G.R., Bergamaschi, B.A., Fram, M.S., Fujii, R., Mopper, K., 2003. Evaluation of specific ultraviolet absorbance as an indicator of the chemical composition and reactivity of dissolved organic carbon. Environ. Sci. Technol. 37 (20), 4702–4708. https://doi.org/10.1021/es030360x.

Wenk, J., Aeschbacher, M., Salhi, E., Canonica, S., von Gunten, U., Sander, M., et al., 2013. Chemical oxidation of dissolved organic matter by chlorine dioxide, chlorine, and ozone: effects on its optical and antioxidant properties. Environ. Sci. Technol. 47 (19), 11147–11156. https://doi.org/10.1021/es402516b.

Westerhoff, P., Mash, H., 2002. Dissolved organic nitrogen in drinking water supplies: a review. J. Water Supply 51 (8), 415–448. https://doi.org/10.1016/S0065-2113(08)60255-2.

Wolfe, R.L., Ward, N.R., Olson, B.H., 1984. Inorganic chloramines as drinking water disinfectants: a review. J. AWWA 76 (5), 74–88. https://doi.org/10.1002/j.1551-8833.1984.tb05337.x.

Zhao, Y., Anichina, J., Lu, X., Bull, R.J., Krasner, S.W., Hrudey, S.E., Li, X.-F., 2012. Occurrence and formation of chloro- and bromo-benzoquinones during drinking water disinfection. Water Res. 46 (14), 4351–4360. https://doi.org/10.1016/j.watres.2012.05.032.

Zimmermann, S.G., Schmukat, A., Schulz, M., Benner, J., von Gunten, U., Ternes, T.A., 2012. Kinetic and mechanistic investigations of the oxidation of tramadol by ferrate and ozone. Environ. Sci. Technol. 46 (2), 876–884. https://doi.org/10.1021/es203348q.